A STUDY OF HYDROGEN ELECTRODIFFUSION IN ALPHA QUARTZ USING ACOUSTIC LOSS TECHNIQUES

By

DAVID WAYNE HART

Bachelor of Science

Southwestern Oklahoma State University

Weatherford, Oklahoma

1984

Submitted to the Faculty of the
Graduate College of the
Oklahoma State University
in partial fulfillment of
the requirements for
the Degree of
MASTER OF SCIENCE
MAY, 1987

A STUDY OF HYDROGEN ELECTRODIFFUSION

IN ALPHA QUARTZ USING

ACOUSTIC LOSS

TECHNIQUES

Thesis Approved:

Joel J. Martin
Thesis Adviser

George S. Weiss

Larry E. Halliburton

Dean of the Graduate College

ACKNOWLEDGEMENTS

I wish to express my sincere appreciation to my committee chairman and adviser, Dr. Joel J. Martin, for his guidance, assistance, and patience throughout this study. I have learned much and have enjoyed working for him the last two years.

I am thankful to my committee members, Dr. George S. Dixon and Dr. Larry E. Halliburton, for agreeing to be on my committee. Also, Charles A. Hunt for his technical assistance over the last two years.

Perhaps the ones most responsible for my accomplishments are my parents, Samuel C. and Delores S. Hart, for their support and help in continuing my education.

Finally, heartfelt thanks to my wife, Debbie, for her love and understanding.

TABLE OF CONTENTS

LIST OF TABLES

LIST OF FIGURES

CHAPTER I

INTRODUCTION

Alpha quartz is a piezoelectric, crystalline form of silicon dioxide that belongs to the trigonal crystal system with point group 32. It is characterized by an axis of three-fold symmetry, commonly called the c or optic axis, and three axes of two-fold symmetry that lie 120^{o} apart upon rotation about the c-axis. Alpha quartz has a density of 2650 kilograms per cubic meter and its hardness is 7 on the Mohs' scale. It exists in both right and left-handed forms and has a phase transition temperature of $573^{o}C$ at atmospheric pressure. Above this temperature it undergoes a phase transition to beta quartz.

The basic structural unit of alpha quartz consists of an SiO_4 tetrahedron with each oxygen atom common to two tetrahedra. Of the four oxygen ions surrounding a silicon there are two types, those with long bonds and those with short bonds. The bond lengths have been measured as 1.612 angstroms for the long bond and 1.606 angstroms for the short bond. The Si-O-Si bond angle is 143.65^{o}. (1,2) Due to its structure, alpha quartz has large channels (~1 angstrom) that run parallel to the c-axis. Because of these channels, ionic conductivity in alpha quartz is very

anisotropic.

Alpha quartz occurs naturally and can be grown hydrothermally from solution. Hydrothermal growth is done in autoclaves at temperatures in the 350^{o}C range and under pressures of 1000 to 1500 atmospheres. This synthetic quartz is usually grown with natural quartz as the starting material. Since quartz is only slightly soluble in water, mineralizers such as sodium hydroxide and sodium carbonate are added to increase solubility. As a result most impurities present in synthetic quartz come from the starting material and the mineralizers.

Defects in Quartz

Two line defects that may occur in alpha quartz as growth or induced defects are optical and electrical twinning. Optical or Brazilian twinning, a growth defect, is the result of right and left-handed regions existing in the same crystal. Electrical or Dauphiné twinning is the result of different regions in a crystal having the same handedness but reversed X axes. Electrical twinning occurs as a growth defect but can be induced by an applied mechanical stress or by cycling the crystal through the phase transition temperature.

Another line defect that occurs upon growth of synthetic quartz are dislocations. These dislocations are usuallly oriented in the direction of growth and are the result of impurities present during growth. The

dislocations give rise to the etch pipe tunnels that form when the crystal is etched during fabrication processes (3).

There are two principle point defects in synthetic quartz. The first gives rise to the infrared absorption bands at 3581, 3437, 3400, and 3348 cm^{-1} wavenumbers. These bands are intrinsic to synthetic quartz, and the intensities of each, relative to each other, appear to be consistent under defect modifying treatments. However, the defect that produces these bands is as yet unidentified, but it is believed to be associated to either the incorporation of a water molecule at oxygen sites or a silicon vacancy that is charge compensated with hydrogen.

The other principle point defect is the substitution of an aluminum atom for a silicon atom at a regular lattice site. The resulting charge imbalance is compensated by either an interstitial alkali ($Al\text{-}M^{+}$), where M denotes a lithium or sodium ion, a proton ($Al\text{-}OH^{-}$) or a hole ($[Al_{e+}]^{o}$). Studies into the concentration of substitutional defects have shown that the substitutional aluminum defect is at least an order of magnitude greater than other substitutional defects in synthetic quartz (4).

The $Al\text{-}M^{+}$ center occurs as a growth defect but the process of electrodiffusion can modify this defect by selectively exchanging the compensating alkalis for other alkalis or protons. The $Al\text{-}OH^{-}$ defect center is usually formed during electron irradiation or hydrogen electrolysis. It consists of a proton bonding to an oxygen ion to form an

OH^- molecule adjacent to a substitutional aluminum. The hole-compensated centers consist of a hole (electron vacancy) trapped in a nonbonding p-orbital of an oxygen ion located adjacent to a substitutional aluminum. If there are sufficient electron traps present in a crystal, this center can be formed by electron or x-ray irradiation. It has also been formed by vacuum electrolysis above the phase transition temperature (5).

Electrodiffusion

Electrodiffusion (sweeping) is a post-growth process used to selectively exchange charge compensating ions in quartz. The interstitial alkalis that compensate for the aluminum lie in the large c-axis channels and are mobile at high temperatures. As a result these alkali ions can be swept along the channels under an applied electric field. The first studies in electrodiffusion were done by King (6), Kats (7), and Fraser (8). They used this process to sweep hydrogen and specific alkalis into quartz. Kreft (5) used this process to sweep holes into quartz by carrying the process in vacuum above the phase transition temperature. Studies into the radiation effects of swept quartz have shown that the radiation hardness is significantly improved if the alkalis in the quartz have been replaced by protons (9,10,11). Other studies, such as those done by Martin *et al.* (12) and Gualtieri and Vig (13), have shown the number density of etch tunnels is lower in hydrogen swept quartz

than in unswept quartz.

The exchange of one alkali for another at the aluminum site is a reversible process but it appears to be irreversible when the alkalis are replaced with protons. Evidence of this can be seen by the infrared spectra of a hydrogen swept sample and a subsequent alkali sweep of the same sample. By monitoring the absorption bands at 3367 and 3306 cm^{-1} wavenumbers, which were suggested to arise from the $Al-OH^-$ center by Kats (7) and were confirmed to be $Al-OH^-$ related by Halliburton *et al.* (14), changes in the $Al-OH^-$ concentration can be detected. A comparison of the infrared spectra after the two sweeps shows no change in the two bands.

The electrodiffusion process is directly related to ionic conductivity. If the alkalis that compensate for the aluminum defect are of one species and are the only charge carriers during the electrodiffusion process, then the conductivity σ can be written, from Jain and Nowick (15),

$$\sigma = (c/2)^{1/2}(ed)^2 N_o f/k \exp(-E/kT). \qquad (1)$$

Where c and N_o are the concentrations of alkali ions and silicon atoms in the crystal, respectively, T the absolute temperature, e the electronic charge, and k Boltzmann's constant. The other factors in the expression are the jump distance d, the oscillation frequency f, and the activation energy of the ion E. The activation energy E is the sum of the association energy of the aluminum-alkali defect and the activation energy for interstitial migration. The factor of

1/2 is included because the aluminum-alkali pair, at least in the case of the aluminum-sodium center (16), has two equivalent orientations.

By combining the exponential prefactors, this expression can be written as

$$\log(\sigma T) = -E/(2.303kT) + \log(A). \qquad (2)$$

With the above expression, a plot of $\log(\sigma T)$ versus $1/T$ yields the activation energy E. Energy values for the sodium ion range from .99eV to 1.25eV and for the hydrogen ion (proton) 1.52eV to 1.95eV. (12,17,18) The energy values are distinguishable from ion to ion but whether the conductivity measured during the electrodiffusion process is due strictly to conduction of the ion from the aluminum defect is questionable since plots of log(σT) versus 1/T will usually yield curved lines.

Electrodiffusion is usually carried out to a maximum temperature in the 450°C to 500°C range with the electric field used to remove the interstial ions applied at room temperature or at the higher temperatures. For all sweeps the electrodiffusion process is carried out in three phases. The first is the region where the sample temperature is increased, the second the region where the temperature is held constant, and the third where the temperature is decreased. By applying the electric field at room temperature and keeping it constant throughout a hydrogen sweep, current measurements yield peaks during the first region, a gradual decrease during the second region, and an

exponential decrease during the third region.

As specific examples, figures 1 and 2 are plots of sample temperature (dashed line) and current (solid line) versus elapsed time of two hydrogen sweeps. The sample in figure 1 has approximately 1 part per million aluminum and the sample in figure 2 has approximately 23 parts per million aluminum.

The third region of each sweep exhibits an exponential decrease in current as a function of temperature. By use of equation 1, calculation of the activation energy of the swept ion is done in this region.

In the second region the current reaches a maximum when the temperature reaches a maximum. Comparison of the two plots shows the maximum current achieved correlates with the aluminum content. Also distinguishable in the plots is a decrease in current over time as the temperature remains constant. Since the mobility of hydrogen is lower than that of the alkalis in quartz, this decay is probably caused by the removal of alkalis from the samples. A comparison of the two plots shows the sharper decrease in currrent also correlates with the aluminum content.

In the first region of each sweep a current peak appears in the 200^{o}C to 375^{o}C temperature range. Though only one peak can be seen here, Hanson (19) has reported as many as seven peaks at various temperatures ranging from 130^{o}C to 500^{o}C. As yet, the source of the current peak shown in the figures 1 and 2 is unknown, but it appears that

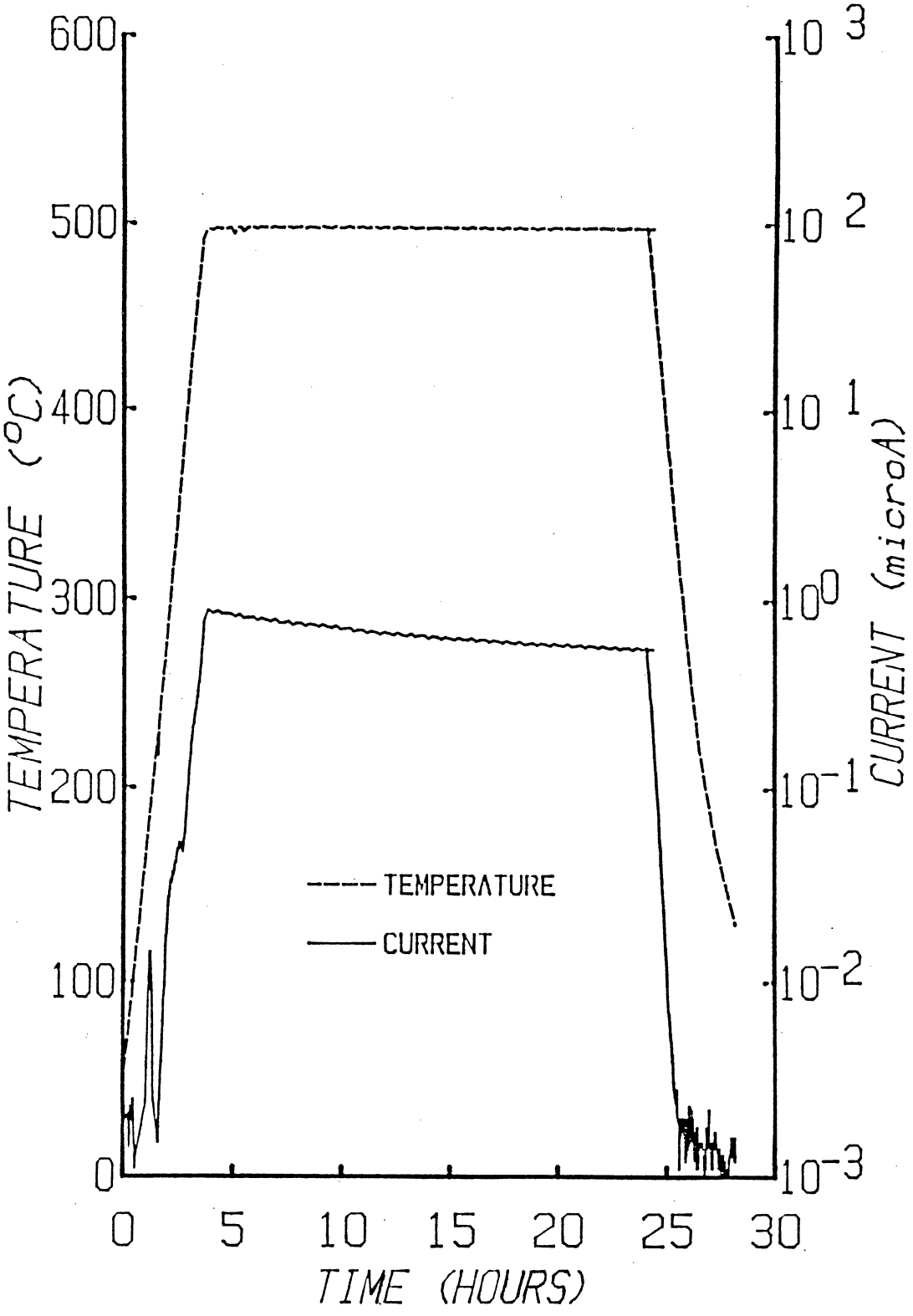

Figure 1. Hydrogen Sweep of an AT-Cut Resonator Containing 1 ppm Aluminum.

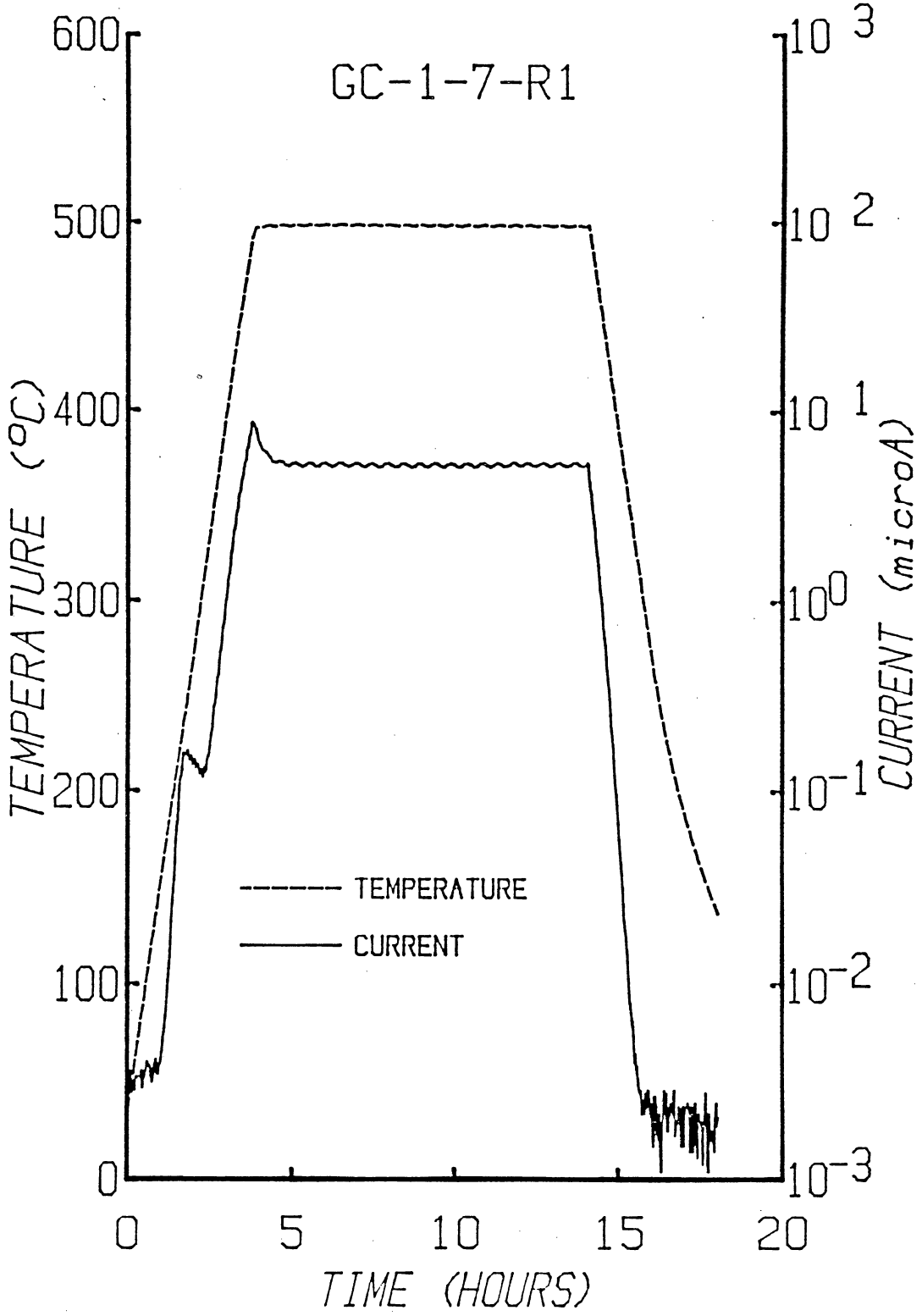

Figure 2. Hydrogen Sweep of an AT-Cut Resonator Containing 23 ppm Aluminum.

the peaks are the result of a thermal release of ions from defects.

Acoustic Loss

Acoustic loss or internal friction arises from the interaction of an applied stress and the resulting strain in piezoelectric, anelastic solids. When a stress is applied to an anelastic solid a new equilibrium condition is achieved, not instantaneously as in the elastic case, but after a sufficient passage of time. For a sinusoidally driven system, the stress will lead the strain by an angle ϕ. By introducing a time dependence into Hookes' law, which equates the stress to the modulus of elasticity and the strain, Nowick and Berry (23) have shown the tangent of this angle can be expressed as

$$\tan(\phi) = \frac{\Delta W}{2\pi W}. \qquad (3)$$

Where ΔW is the energy dissipated per unit volume in a full cycle, and W is the maximum stored energy per unit volume. The above expression gives the quantity commonly called the internal friction or acoustic loss and is equal to the inverse of the quality factor Q of a vibrating system.

In the case of point defects, thermally activated hopping of atoms or defects between equivalent sites gives rise to an increase in the acoustic loss. When measured, the loss exhibits peaks where the internal friction increases above a background whose origin are the phonon-phonon interactions that are inherent in all solids. These

peaks are in the form of Debye peaks and can be expressed as (23),

$$\tan(\phi) = \frac{D\ \omega\tau}{(1+\omega^2\tau^2)} . \qquad (4)$$

Where D is the "relaxation strength", ω the angular frequency, and τ the relaxation time of the defect. Measurement of the acoustic loss using this expression can be done by varying the frequency while keeping the relaxation time constant or by varying the relaxation time and while keeping the frequency constant. Both methods require numerous resonators operating on different frequencies or the capability of one resonator to operate on more than one frequency.

The measurement of acoustic loss or internal friction aids in the identification of the defects that produce anelasticity in crystalline solids. Acoustic loss measurements also give insight into the effects of defect modifying treatments such as electrodiffusion and electron or x-ray irradiation. The earliest study in low temperature (<100K) acoustic loss was done by Bommel et. al. (20,21) on an AT-cut 5 megaHertz quartz resonator. During the investigation two acoustic loss peaks were found, one near 20K and the other near 50K. The 50K loss peak was found to have an activation energy of .0565 eV and a relaxation frequency of 6×10^{12} per second. King (6,22) found that seed orientation during growth of synthetic quartz had an effect on the 50K peak and discovered another loss peak near 135K

in samples that had a large 50K peak. He also found that the 50K loss peak could be described by a single relaxation process and that x-ray irradiation and electrolysis could remove the peak. In 1964, Fraser (8) used electrodiffusion to sweep lithium, sodium, and potassium into quartz samples. A measurement of the acoustic loss of these samples indicated the 20K loss peak was not alkali related while the 53K loss peak was sodium related. The model of the defect proposed, and later accepted, to produce the 53K loss peak was the $Al\text{-}Na^{+}$ defect center.

High temperature loss measurements (>300K) done on natural and synthetic quartz sample were also presented by Fraser (8). The loss spectra of unswept samples were found to increase exponentially as the sample temperature reached 150°C-200°C and retained the exponential character up to near the phase transition temperature. This exponential increase was thought to be the result of thermally activated ions. Subsequent hydrogen sweeping of the samples resulted in a decrease of the exponential loss and produced a peak near 300°C. Though a number of loss peaks have been found ranging from near the 20K peak to the phase transition temperature only the 53K peak and the high temperature loss peak(s) are in the scope of this study.

The two methods used in this study to measure the acoustic loss (Q^{-1}) versus temperature are the logarithmic decrement and the transmission techniques. Both are resonance methods and make use of different properties of

quartz resonators.

The basis of the logarithmic decrement method is to pulse the resonator at its resonant frequency for a short period of time then allowing the oscillations to freely decay. When a resonator is stressed sinusoidally at its resonant frequency the converse piezoelectric effect causes a strain in the crystal that varies with the stress. Upon removal of the stress, the crystal mechanically relaxes and, much like an under-damped oscillator, overshoots its equilibrium position to a position of maximum strain in the opposite direction. The relaxation induces a measurable alternating voltage on the electrodes at the same frequency as the mechanical oscillations that will eventually decay to zero. The differential equation that describes the decay can be written, (23)

$$m\ddot{x} + K_1 (1+i\tan\phi)\, x = 0. \qquad (5)$$

Where m is the mass attached to the end of an anelastic spring having force constant $K_1(1+i\tan\phi)$.

The solution of equation 5 which describes the free vibrations in the presence of internal friction is of the form, for $\phi<<1$,

$$x = x_o \exp(-\omega_o \phi t/2) \exp(i\omega_o t),$$

where ω_o, the frequency in the absence of anelasticity, is given by $(K_1/m)^{1/2}=2\pi f_o$. With f_o the resonant frequency of the crystal. The induced voltage will decrease exponentially as

$$V = V_o \exp(-t/t_o) \exp(i\omega_o t),$$

where t_o is the time constant of the decay and is equal to $t_{1/2}/\ln(2)$. A comparison of the damping terms in x and V shows

$$\omega_o \phi/2 = 1/t_o$$

or,

$$\phi = 1/(\pi f_o t_o).$$

By substituting for t_o, the expression for the acoustic loss becomes,

$$Q^{-1} = \ln(2)/(\pi f_o t_{1/2}). \qquad (6)$$

Hence, by pulsing the resonator at frequency f_o then detecting, amplifying, and then rectifying the decaying signal, a measurement of the time for the decaying signal to fall to half its initial value yields the acoustic loss.

The transmission method makes direct use of the electrical equivalent of the quartz resonator. Shown in figure 3, this circuit consists of an inductor, a capacitor, and a resistor in parallel with a second capacitor. The inductance L, the capacitance C, and the resistor R, are the crystal parameters and the capacitance C_o is due to the electrodes and cables connecting the quartz resonator to any apparatus. This circuit exhibits two resonant frequencies. One of minimum impedance (series resonance) and the other of maximum impedance (parallel resonance). For purposes of measuring the acoustic loss of the crystal, the series resonant frequency is used.

Using electrical analysis the Q of a series-resonant RCL circuit is found to be given by

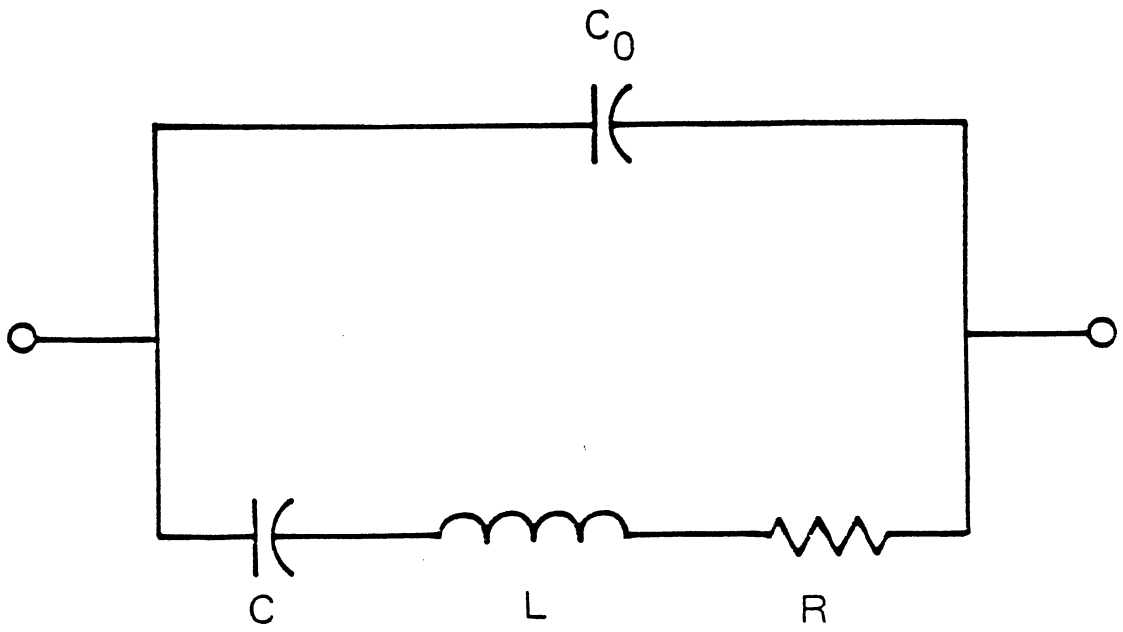

Figure 3. Electrical Equivalent of a Quartz Resonator.

$$Q=\omega L/R \tag{7}$$

Thus, the acoustic loss can be obtained by measuring the equivalent series resistance and the inductance of the resonator.

The transmission method consists of placing the resonator in a pi-network, shown in figure 4, to measure both parameters needed to obtain the acoustic loss. At resonance the phase difference at points A and B of the pi-network is zero, and a measurement of the voltage amplitudes at these two points yields the resistance R of the crystal by

$$R=\frac{R_2R_eR_L}{(R_1+R_2)(R_L+R_1)}\frac{V_a}{V_b}-R_e-R_T. \tag{8}$$

With

$$R_e=\frac{R_2(R_1+R_1)}{R_2+R_1+R_1}$$

and

$$R_T=\frac{R_1R_2}{R_1+R_2}.$$

The inductance is found by incrementing the frequency about the series resonant frequency and obtaining the impedence of the crystal. With the reactance X given by

$$X=4\pi\delta L, \tag{9}$$

where δ is the incremental frequency, a plot of the impedence versus frequency yields a straight line with a slope of $4\pi L$. Equations 8 and 9 are derived in the appendix and follow calculations done by Martin and Wilson. (24)

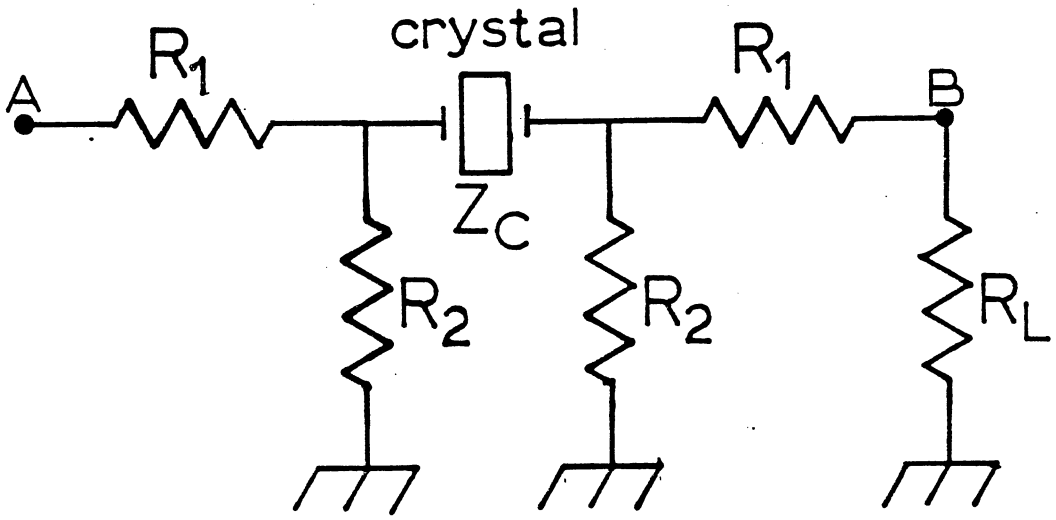

Figure 4. Pi-Network of the Acoustic Loss Transmission System.

Purpose of Investigation

The purpose of this study was to investigate the replacement of thermally activated alkalis for protons during hydrogen electrodiffusion. By correlating ion current, infrared absorption, and acoustic loss measurements this study is an attempt to establish the origin of the current peak seen during the warmup phase of hydrogen electrodiffusion.

CHAPTER II

EXPERIMENTAL TECHNIQUES

Electrodiffusion

The basic process of electrodiffusion is to apply an electric field across a sample at elevated temperatures. With this process, interstitial ions present in the quartz sample can be removed or selectively exchanged.

A block diagram of the sweeping facilities is shown in figure 5. The sample is connected in series with a power supply and a 1000 ohm standard resistor. The power supply-a Hewlett-Packard (HP) 59506A power supply programmer or a KEPCO APH 2000M-is connected to the sample holder by RG-58 coaxial cable. For a required voltage greater than ten volts the KEPCO power supply is used.

The sample holder is made of graphite and stainless steel. The sample rests between a graphite button on the negative side and a graphite electrode on the positive side. The arms that extend the sample into the furnace are made of stainless steel tubing and are insulated from each other with a ceramic spacer. The holder rests inside a silica tube inserted into the furnace, and a gas inlet valve is present to vary the atmosphere in the chamber. The pressure

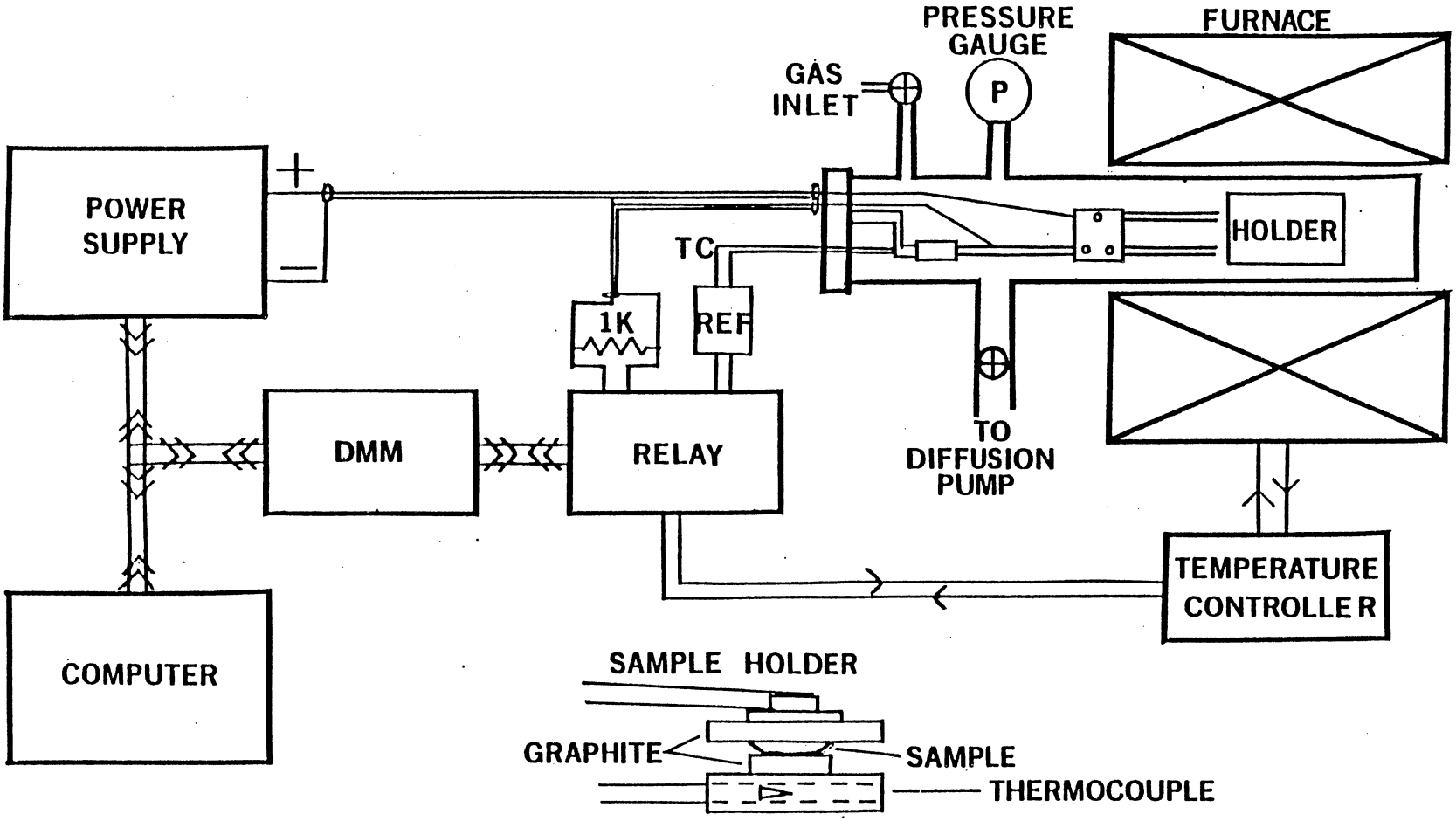

Figure 5. Block Diagram of Electrodiffusion System.

inside the chamber is monitored with the pressure gauge.

During the electrodiffusion process, the time elapsed from the start of the process, the sample temperature, and the current are measured and stored by the computer. The computer, an HP 86, is interfaced via the HP interface bus to the relay, the power supply programmer, and an HP 3478A digital multimeter. The computer controls the HP 59306A relay box so that either the thermocouple or the standard resistor signals are read by the DMM. Current measurements are obtained by measuring the voltage drop across the standard resistor, and the sample temperature is measured with a Type K (chromel-alumel) thermocouple which is positioned directly below the sample. The computer controls the sample temperature by controlling the furnace through the temperature controller.

Figure 6 shows a flow chart of the program used to control the process, and a plot of the temperature curve versus time elapsed is shown in figure 7. The entered parameters are the maximum temperature desired (TMAX), the applied voltage (V), time between data points as the temperature is increasing and decreasing (W1), and time between data points as the temperature is held constant (W2). The sample area (A) and thickness (th) are also entered.

The program allows 400 data points throughout the process with each point consisting of the time elapsed, the current, and the temperature. The applied voltage and the

sample area and thickness are also stored. The temperature of the sample is increased at a rate of 2°C per minute, and during this time the current, temperature, and time are taken at the specified intervals W1. As the temperature becomes greater than or equal to TMAX the temperature is either held constant or decreased depending on the value of W2. If W2 is greater than zero, then the temperature is held constant and 100 data points are taken at intervals of W2. If W2 is equal to zero, then the temperature is decreased at a rate of 2°C per minute and data are taken at intervals of W1.

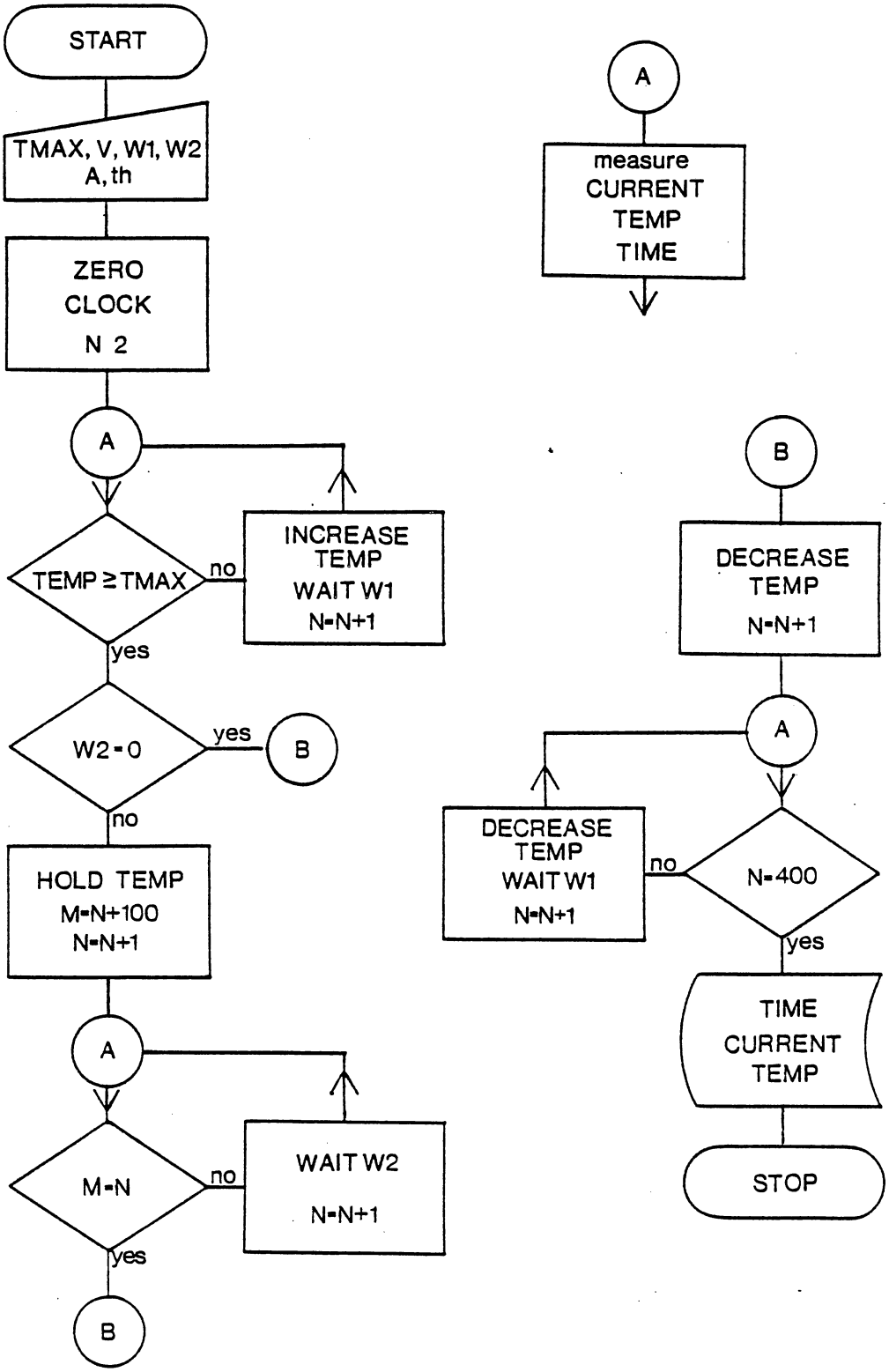

Figure 6. Flow Chart of Program Used to Control the Electrodiffusion Process.

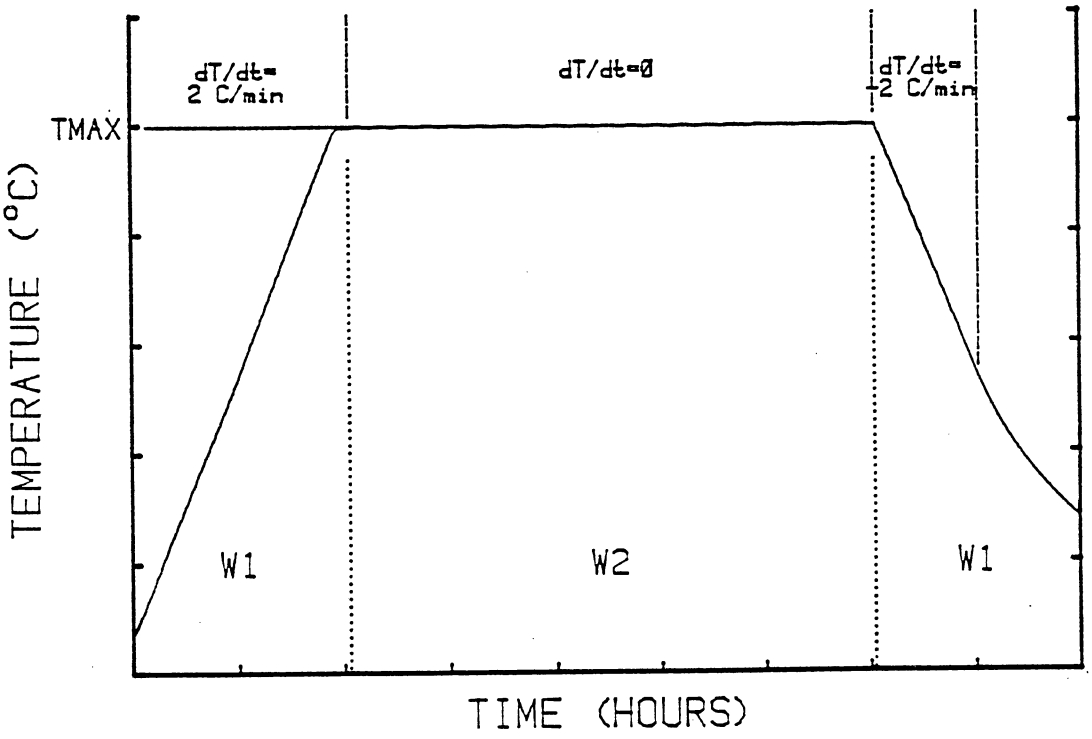

Figure 7. Temperature Profile of Electrodiffusion Process.

Acoustic Loss: Logarithmic Decrement Technique

The logarithmic decrement system used in this study is shown in figure 8. The advantages of using this system are that the acoustic loss can be measured as high as 10^{-4} and that the measurements can be done with the sample placed in a gap holder or with electrodes vapor deposited onto the resonator surfaces.

The computer, an HP 87, is connected to the experimental apparatus via the HP interface bus and is used in the aquisition of the sample temperature and the parameters to calculate the acoustic loss. The other apparatus that make up this system are an HP 3325A frequency sythesizer, an HP 5326A timer-counter, an HP 3478A digital multimeter (DDM), a Tektronix 5441 storage oscilloscope, a temperature controller, and a logarithmic decrement (log-dec) receiver. The receiver was designed and built at Oklahoma State University by Professor J. J. Martin and given the designation Model 13 ESR. The temperature controller, which consists of a heater/furnace and temperature measuring device, is altered according to the temperature region in which the acoustic loss is measured.

With this system, the resonator is driven by the frequency synthesizer at its resonant frequency f_o ($f_o \cong 5$MHz) and allowed to freely decay. The crystal can be driven for 10-40 milliseconds every .5, 1, 2, or 5 seconds. Most data is taken at a 1 second repetition rate.

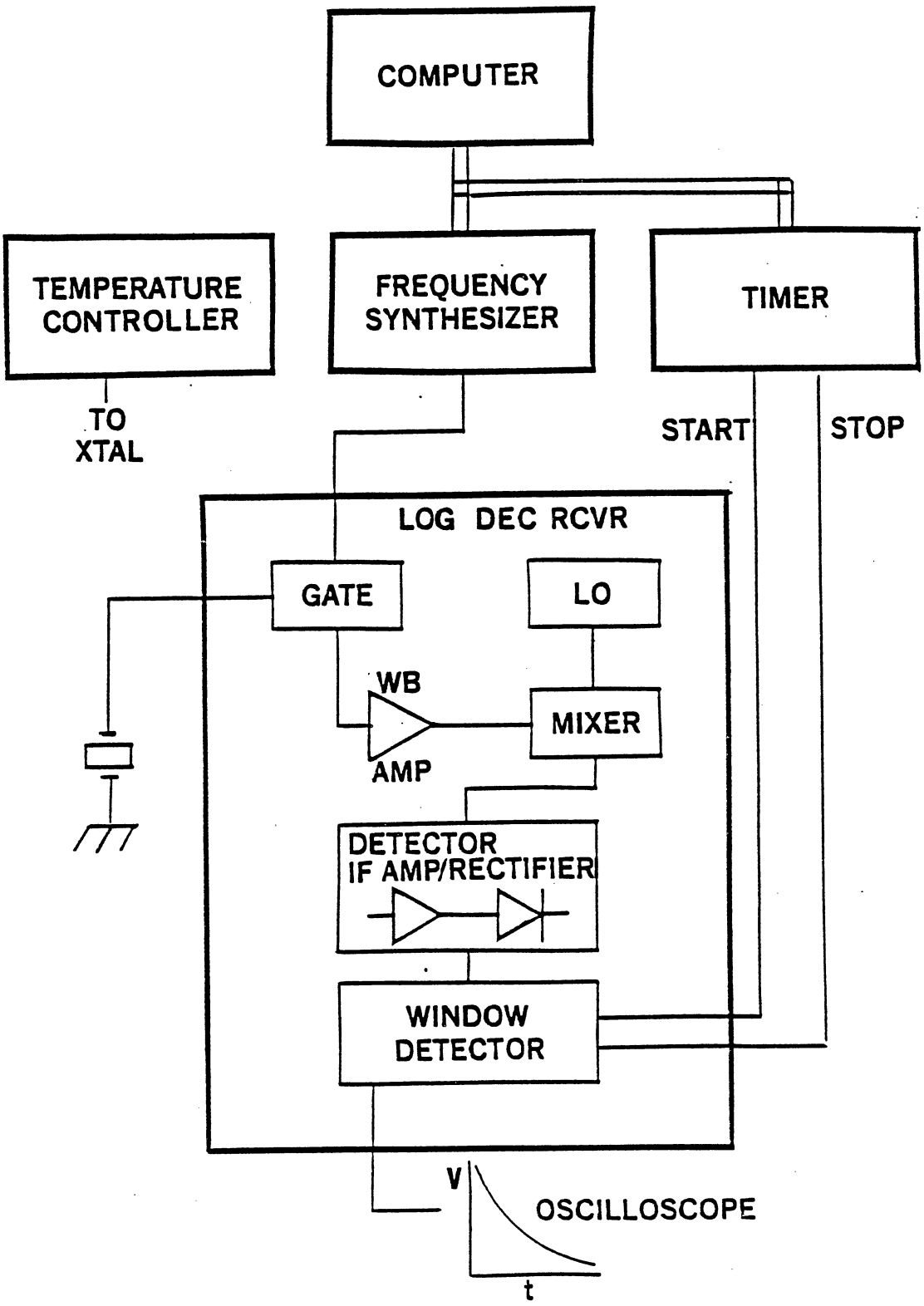

Figure 8. Acoustic Loss Logarithmic Decrement System.

The decaying radio frequency (rf) signal is at frequency f_o, and the decay envelope is exponential in character. This signal is fed back through the gate, into a wide-band amplifier, and then into a double balanced mixer. Here the signal is mixed with the local oscillator (LO) signal of $f_o \pm 445$ kHz. The output from the mixer is an intermediate frequency (IF) of 445 kHz which is detected and amplified by a precision rectifier circuit. The rectified IF signal, which has a maximum of 12 volts, is displayed on the storage oscilloscope and is sent to the window detector. The window detector starts the counter as the decaying signal falls to 8 volts and stops the counter as the signal falls to 4 volts. The counter then gives the time constant $t_{1/2}$ of the decay.

Tuning of the resonator to its resonant frequency is done manually with the frequency adjusted so that the decay, which is displayed on the oscillope, is at maximum amplitude. Output to the computer consists of the resonant frequency, the time constant of the decay, and the temperature of the sample. The computer calculates the acoustic loss using equation 6.

Acoustic Loss: Transmission Technique

This alternative method of measuring acoustic loss measures the motional resistance and inductance of the quartz crystal and is used over the temperature range 8K to 320K. Though it can only measure the resistance up to a

calculated acoustic loss of $5x10^{-5}$ it has an advantage over the log- decrement system in that it is almost fully automated.

As shown in figure 9, the system consists of an HP Integral Personal Computer, an HP 3325A frequency synthesizer, an HP 5316A counter, an HP 3338A DVM, a TRI Research T-2000 temperature controller, and an HP 59307A relay on the control rack. The refrigerator rack consists of an HP 5405A vector voltmeter, a CTI-Cryogenics closed-cycle helium refrigerator, and a pi-network. The components of the control rack are connected to the computer by the HP interface bus while the connections to the pi-network and the vector voltmeter are made with RG-58 coaxial cable.

With the voltage at point A (V_a) of the pi-network relatively constant over the temperature range in which the resistance is measured, the VVM measures the voltage (V_b) and phase with respect to point A at point B. At the resonant frequency of the crystal, the phase difference between points A and B is zero and the motional resistance of the crystal is then found by

$$R=4(V_a/V_b)-28.$$

With the values of R_1, R_2, and R_L of the pi-network chosen to be 30, 20, and 50 ohms, respectively.

With the phase signal fed to the DVM, the resonator is tuned to its resonant frequency by use of a feedback loop as shown in figure 10. The computer reads the phase and the current frequency then calculates the frequency needed to

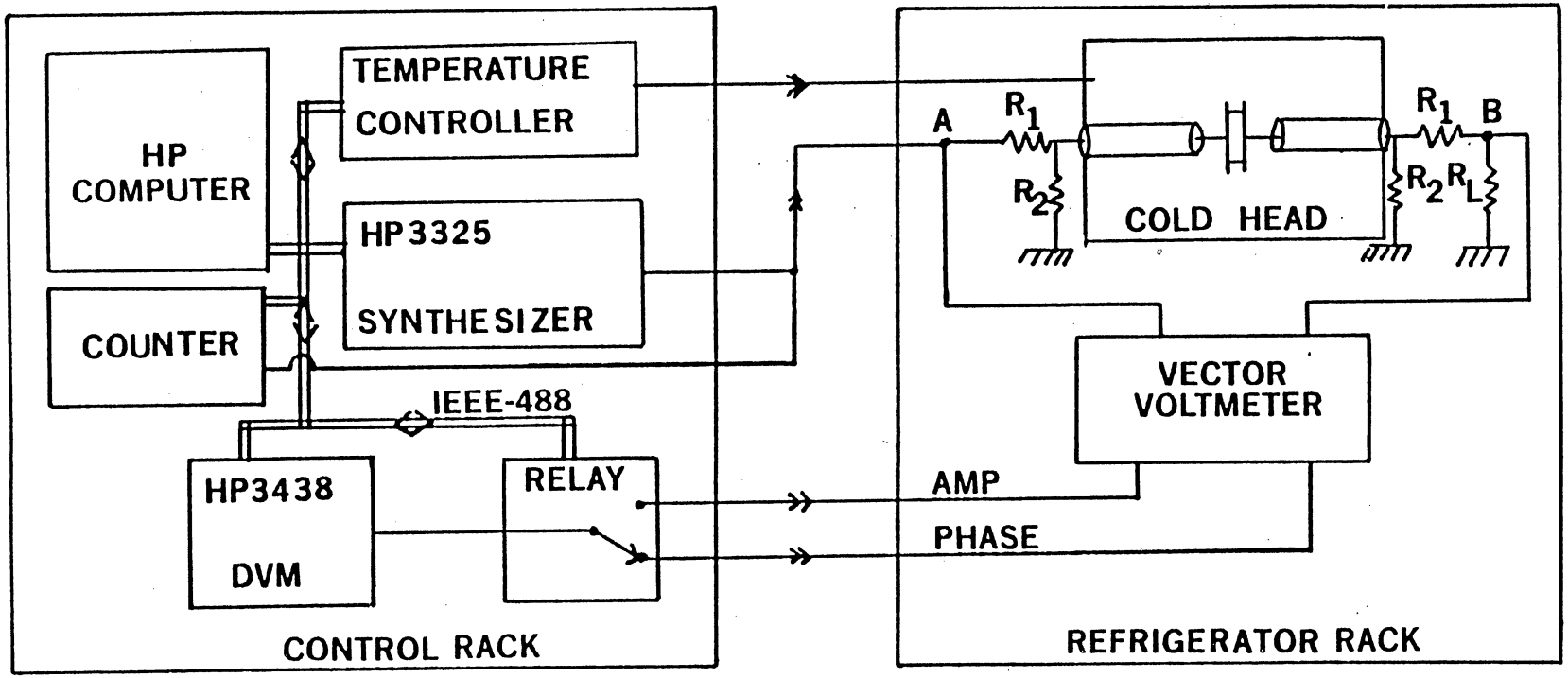

Figure 9. Acoustic Loss Transmission System.

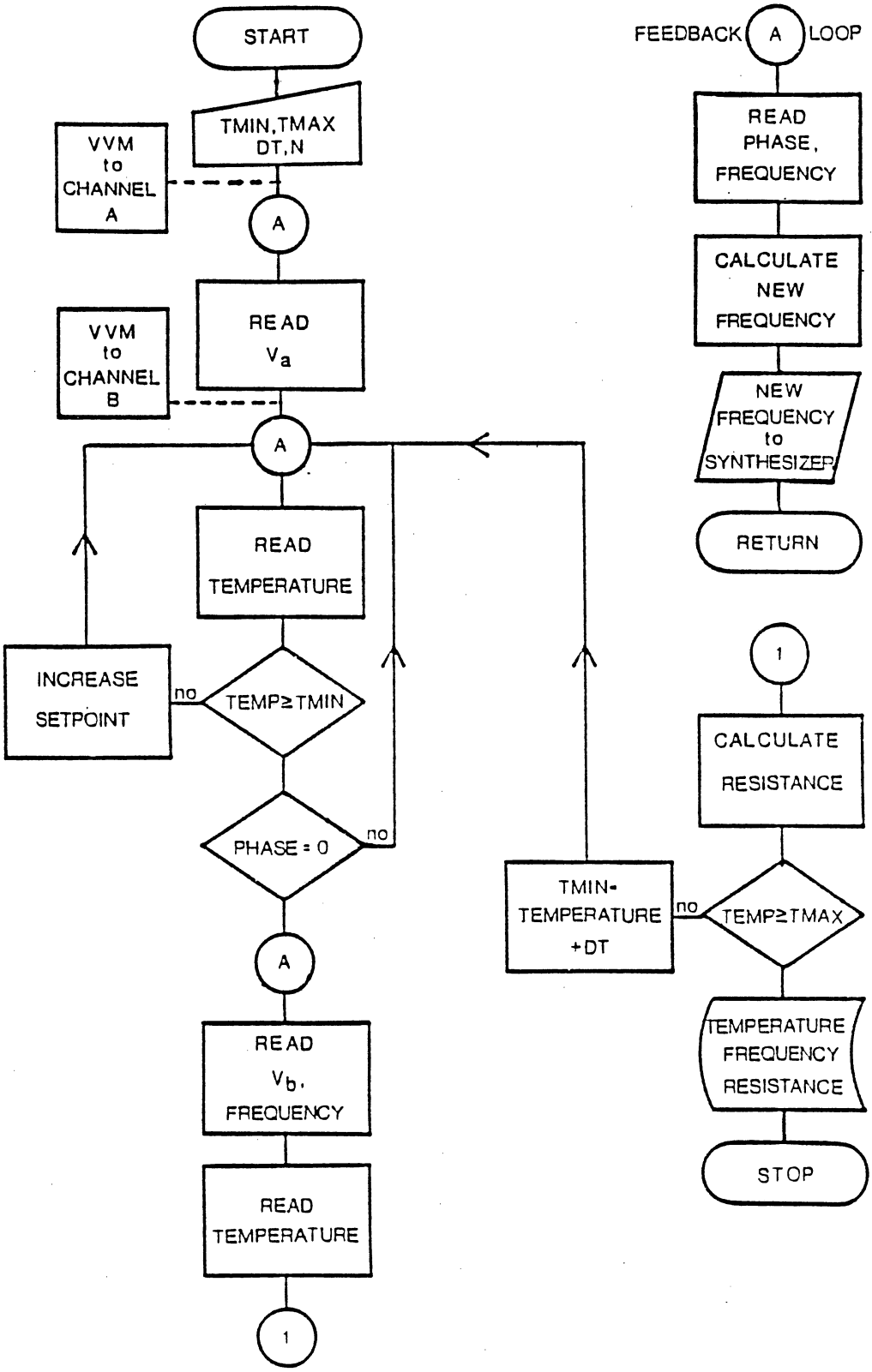

Figure 10. Flow Chart of Program Used to Control Transmission System.

reduce the phase to zero. The new frequency is sent to the synthesizer and the process is repeated N times. The program shown in the same figure makes use of the feedback loop to obtain the temperature and series resistance of the resonator. The entered parameters are the minimum (TINC) and maximum (TMAX) of the temperature range over which the data are to be taken. The temperature interval (DT) between data points and the number of times (N) the feedback loop repeats itself are also entered.

The program requires the operator to switch the VVM to channel A so that V_a is outputted to the relay. The resonator is then tuned to frequency and the relay is triggered to output V_a to the DVM where it is read by the computer. The program is then paused and the VVM is switched to channel B. Continuation of the program results in tuning the resonator to its resonant frequency and increasing the sample temperature by increasing the setpoint on the temperature controller until the desired temperature (TINC) is reached. When TINC is reached, and the phase is equal to zero, the computer triggers the counter to read the frequency and the temperature controller to read the sample temperature. The relay is triggered to output V_b to the DVM and the temperature is read again. The computer then reads V_b from the DVM and the frequency from the counter and averages the temperatures. The resistance is calculated and the sample temperature is compared to TMAX. If the sample temperature is less than TMAX, then the computer increases

TINC by DT and returns to the feedback loop.

After accumulation of the resistance data the acoustic loss is found by

$$Q^{-1}=R/\omega L.$$

The value of the inductance L is found as shown in the appendix and the angular frequency $\omega=2\pi f_o$ (f_o is the resonant frequency of the crystal). From 8K to 320K, f_o changes at most by 6kHz. Since this is a small change, compared to 5MHz, the value of the inductance found at room temperature is used throughout the acoustic loss calculations.

CHAPTER III

EXPERIMENTAL PROCEDURE

Sample Description

The two sets of samples used in this study consisted of 5MHz AT-cut 5th overtone resonators cut from pure z-growth lumbered bars of synthetic quartz. The first set consisted of only one resonator and was given the designation D14-45. The lumbered bar from which this resonator was taken was grown by Sawyer Research Products (25) and contains less than 1 part per million aluminum. (26) It was fabricated by Piezo Crystal Company (27) following specifications by Warner (28) and has a Q value of 1.8 million at room temperature. The second set, consisting of two GC-1-7 samples, was grown by Motorola (29) and contain approximately 23 parts per million aluminum. This set was fabricated by KW Manufacturing (30) following specifications by Warner (28) and have room temperature Q values ranging from 1.3 million to 1.6 million.

Since only one resonator was designated D14-45, any reference to this resonator will be made by calling it D14-45. However, since two GC-1-7 resonators are used in this study, reference to a particular GC-1-7 resonator will be

done by referring to it as GC-1-7-R#. Using this notation, GC-1-7-R1 refers to resonator number one of the set GC-1-7.

Sample Preparation and Mounting

Deposition of electrode material on the surface of the sample is a requirement for electrodiffusion and the measurement of equivalent series resistance. In each case the resonator is a component of an electrical circuit. The electrode material makes a good electrical contact with the sample, and for electrolysis acts as an equipotential surface.

The gold electrode material used in this study was deposited by passing a current through a tungsten filament wrapped with gold wire. Before the gold was deposited, the resonators were immersed in an ultrasonic cleaner with water and a laboratory cleaning fluid as the cleaning solution until water beaded on its surface. The resonators were then baked above 100°C for at least thirty minutes.

For a sample undergoing alkali electrodiffusion a salt was deposited on one surface of the sample by evaporation from a tungsten boat. A gold film was then plated over the salt and another gold film, comprising the second electrode, was then deposited on the opposite side of the sample. For hydrogen sweeps only a gold film was deposited on both faces of a resonator. All depositions were carried out at pressures on the order of 10^{-6} Torr to reduce contamination from the laboratory air and to prevent burning out the

filament.

Throughout most of this study, the D14-45 resonator was mounted in an HC-40 holder. The electrode configuration for this resonator was easily managed by placing the resonator in a mask made by Fotofabrication. (31) The electrodes were deposited so that they lay along the direction perpendicular to the X axis. The joining of two holder leads with the electrodes of the resonator was accomplished by using a silver bearing polyimide adhesive compound.

Electrodiffusion Procedure

After the sample was coated, it was inserted between the two graphite electrodes that make up part of the sample holder. In the case of an alkali sweep the salted side was oriented so that it was in contact with the positive cathode. The holder was then inserted into the temperature controlled tube furnace, sealed airtight, and placed under vacuum for at least an hour before the actual electrodiffusion process began. This was necessary to remove adsorbed gases; the pressure attained was on the order of 10^{-6} Torr. For alkali sweeps the sweeping process was carried out under vacuum and for hydrogen sweeps a hydrogen atmosphere was introduced into the chamber.

The electric field across the sample was typically 30 volts per centimeter for alkali sweeps and 2000 volts per centimeter for hydrogen sweeps. The difference in the electric fields is due to the lower mobility of hydrogen in

quartz compared to the alkalis. The measured (calculated) electric field is relative to the center of the resonator. The electric field was applied at room temperature and kept constant throughout the process.

High Temperature Acoustic Loss Measurements

High temperature (>300K) acoustic loss measurements using the log-decrement technique were done before, during, and after the hydrogen sweeping of D14-45 to compare the acoustic loss with the experiments done by Fraser. (8)

These measurements were done by connecting the log-decrement receiver to the positive lead of the power supply of the electrodiffusion apparatus. Isolation of the receiver from the power supply was achieved by placing an rf transformer and a capacitor in series with the crystal, and a 10K resistor was used to isolate the rf signal from the output of the power supply. A capacitor was also inserted before the 1K resistor of the electrodiffusion system to ground the rf signal. The silica furnace tube of the electrodiffusion system was replaced with a stainless steel tube to provide adequate shielding, and the negative electrode was insulated from the tube with ceramic.

Low Temperature Acoustic Loss Measurements

The low temperature (<300K) acoustic loss measurements were done by obtaining the equivalent series resistance of the resonator using the transmission technique.

After the sample was mounted in an HC-40 holder, it was inserted into the cold head and placed under vacuum for at least an hour. During this time the resonant frequency, inductance, and the equivalent series resistance at room temperature were found. When the resistance was anomalously high, indicating poor electrical contact, the sample was taken out, cleaned, and mounted again. The cold head was then sealed from the vacuum system and the helium refrigerator was turned on. The cooling time is approximately 1.5 hours and during this time the resonator was kept at resonance with the feedback loop discussed in Chapter 2.

Resistance data was taken from 8K to the maximum-desired temperature using the program discussed in Chapter 2. After the computer obtained the first data point, the program was paused and the heater voltage was increased to maximum. This usually resulted in a temperature rise of not more than 10 degrees, and the sample was allowed to cool before continuing.

Statement of Errors

The sample temperature was measured during the electro-diffusion and high temperature acoustic loss experiments through use of a Type K thermocouple. Because of the uncertainty of the thermocouple ($\pm 2^{o}C$) and the location of the sample away from the thermocouple, the sample temperature will differ from the thermocouple temperature.

This temperature difference can be as much as 10°C during an alkali sweep and will be small during a hydrogen sweep.

The sample in the cold head of the transmission system is enclosed in aluminum at the end of an aluminum cylinder while the temperature sensor is located inside a copper disk attached to the cylinder. Resistance data taken with this system shows good temperature agreement at low temperatures when the heating rate of the sensor is about half a degree per minute. As will be seen by the location of the 53K loss peak in graphs to be shown later, the peak appears to be centered within two degrees of 53K.

The calculation of the acoustic loss with both the transmission and log-decrement systems assumes only the crystal parameters contribute to the loss. In both cases the parallel capacitance and the loss due to the mounting of the crystal are neglected. Since the loss obtained at 8K for most samples indicates Q values on the order of 10^{-8}, the loss due to the mounting of the crystal is assumed to be small at all temperatures.

With the log-decrement system, the resonant frequency of the crystal can be found within a range of 5Hz. Since this range is small compared to 5MHz, this does not effect the acoustic loss values. The main contribution to error in the log-decrement system, neglecting error in the log-decrement receiver, is the time constant $t_{1/2}$. This time constant has an uncertainty of ±1.5% at 65ms and ±0.5% at 10ms. Therefore, a modest estimate of error in the loss

measured with this system is 5%.

Obtaining the acoustic loss with the transmission system relies on the value of the series resistance. This parameter is calculated using the values of the resistors of the pi-network, which have a tolerance of 1%, and the measured value of V_b. Before the computer retrieves V_b, the temperature is still increasing and the resonant frequency of the crystal is not adjusted to compensate for the resulting deviation from zero phase. The deviation from zero phase is about 15 degrees resulting in an error in V_b of about 10%. For this system, a 15% error is estimated on the calculated loss.

CHAPTER IV

RESULTS AND DISCUSSION

A series of hydrogen sweeps was performed on a sodium swept GC-1-7-R4 and the D14-45 samples to temperatures which ranged through the current peak's temperature range. During the hydrogen sweeping of the D14-45 sample the acoustic loss was measured by the logarithmic decrement method to observe any changes in the loss at the higher temperatures. After each sweep on D14-45, the 53K Al-Na^+ acoustic loss peak was measured by the transmission method to determine the temperature at which the sodium ions are swept out of the sample. For comparison with the GC-1-7-R4 sample used in this study, GC-1-7-R1 was hydrogen swept (figure 2) for 10 hours at 500°C under an applied electric field of 2000 volts per centimeter.

Table I lists the maximum temperature achieved for each sweep of GC-1-7-R4. For each sweep an electric field of 2000 volts per centimeter was applied at room temperature. The current density for this series of sweeps is plotted versus temperature in figure 11 with the current density of the hydrogen sweep, done after sodium sweeping, of GC-1-7-R1 included. Here, the maximum current density achieved clearly outlines a peak similar to that of GC-1-7-R1 and

increases above the peak in a manner also similar to the GC-1-7-R1 sample. For the higher temperature sweeps, sweeps 10 and 11, the current does not increase until the sample temperature has reached the maximum temperature range of the current peak. This is characteristic of hydrogen sweeping and is an indication that all the ions responsible for the peak have been swept out of the sample.

TABLE I

HYDROGEN SWEEPS
OF GC-1-7-R4

SWEEP NUMBER	TEMPERATURE (^{o}C)
1	198
2	223
3	248
4	272
5	294
6	320
7	344
8	375
9	397
10	424
11	446

Table II lists the activation energies, calculated from data taken during the cooldown of the sample, of each sweep and the energy values for hydrogen and sodium reported by Martin (12), Verhoogan (17), and Wendon (18). This data

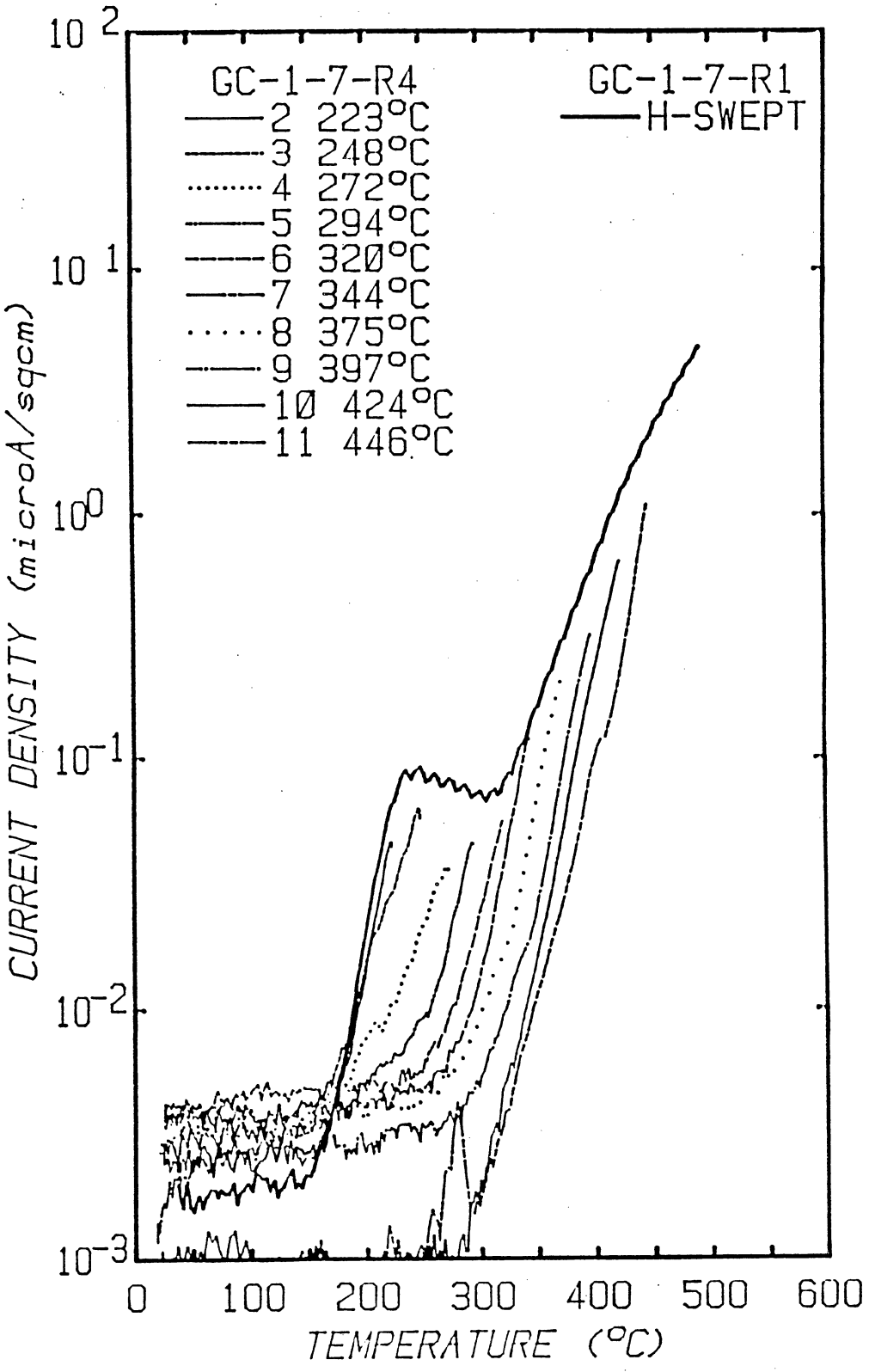

Figure 11. Current Density Versus Sample Temperature of GC-1-7 Hydrogen Sweeps.

shows an increase to hydrogen-like values as the sweeping temperature increases but does not yield information about dissociation. Interpretation of this data is furthur complicated by the fact that more than one ion source may contribute to the conductivity.

TABLE II

CALCULATED ACTIVATION ENERGIES
OF HYDROGEN SWEEPS ON GC-1-7-R4

Maximum Sweeping Temperature (^{o}C)	Activation Energy (eV)
440	1.86
415	1.94
390	1.79
365	1.87
344	1.70
320	1.50
294	1.46
272	1.31
248	1.13
223	1.31
198	0.92

Martin, Na^{+} .99-1.25 eV, H^{+} 1.52-1.95 eV
Verhoogan, Na^{+} 1.03-1.2 eV
Wendon, H^{+} 1.71-1.75 eV

Table III lists the absorption of the 3367 cm^{-1} waveband that is associated with the Al-OH^{-} defect center (14) and the absorption of this same waveband of the

hydrogen swept GC-1-7-R1 sample. These measurements were taken on a Beckman Model IR 4240 infrared spectrophotometer with the x axis of the resonator blank vertical. This data shows no increase in the strength of the 3367 cm^{-1} waveband and indicates that exchange of sodium ions for protons at the aluminum defect site did not occur.

TABLE III

INFRARED ABSORPTION OF THE 3367 cm^{-1} WAVEBAND OF GC-1-7-R4

TEMPERATURE (°C)	ABSORPTION
320	.007
294	.007
248	.006
223	.006
197	.006
HYDROGEN SWEPT GC-1-7-R1	.31

A series of nine hydrogen sweeps were done on the unswept D14-45 sample. The maximum temperature and applied electric field of this series are shown in Table IV. Except for the last three sweeps, the sample was mounted in the HC-40 holder. The applied electric field was 1250 volts per centimeter, unless otherwise indicated, and the high temper-

ature acoustic loss was measured during the electrodiffusion process on sweeps 1 through 7 as described in Chapter III. For sweeps 1 through 6 the sample temperature was immediately decreased after reaching the stopping temperature. On sweeps 7 through 8 the temperature was held constant for the specified times. After each sweep the acoustic loss was obtained from 8K to 100K using the transmission method.

TABLE IV

HYDROGEN SWEEPS OF D14-45

SWEEP NUMBER	MAXIMUM TEMPERATURE (^{o}C)	APPLIED ELECTRIC FIELD (V/cm)
1	216	1250
2	261	1250
3	305	1250
4	355	1250
5	404	1250
6	453	1250
7	460	1250/2000[1]
8	459	1250[2]
9	459	1250[3]

[1]Field increased during temperature hold of 18 hours.
[2]Temperature hold of 10 hours.
[3]Temperature hold of 20 hours.

Figure 12 shows the initial high temperature loss taken

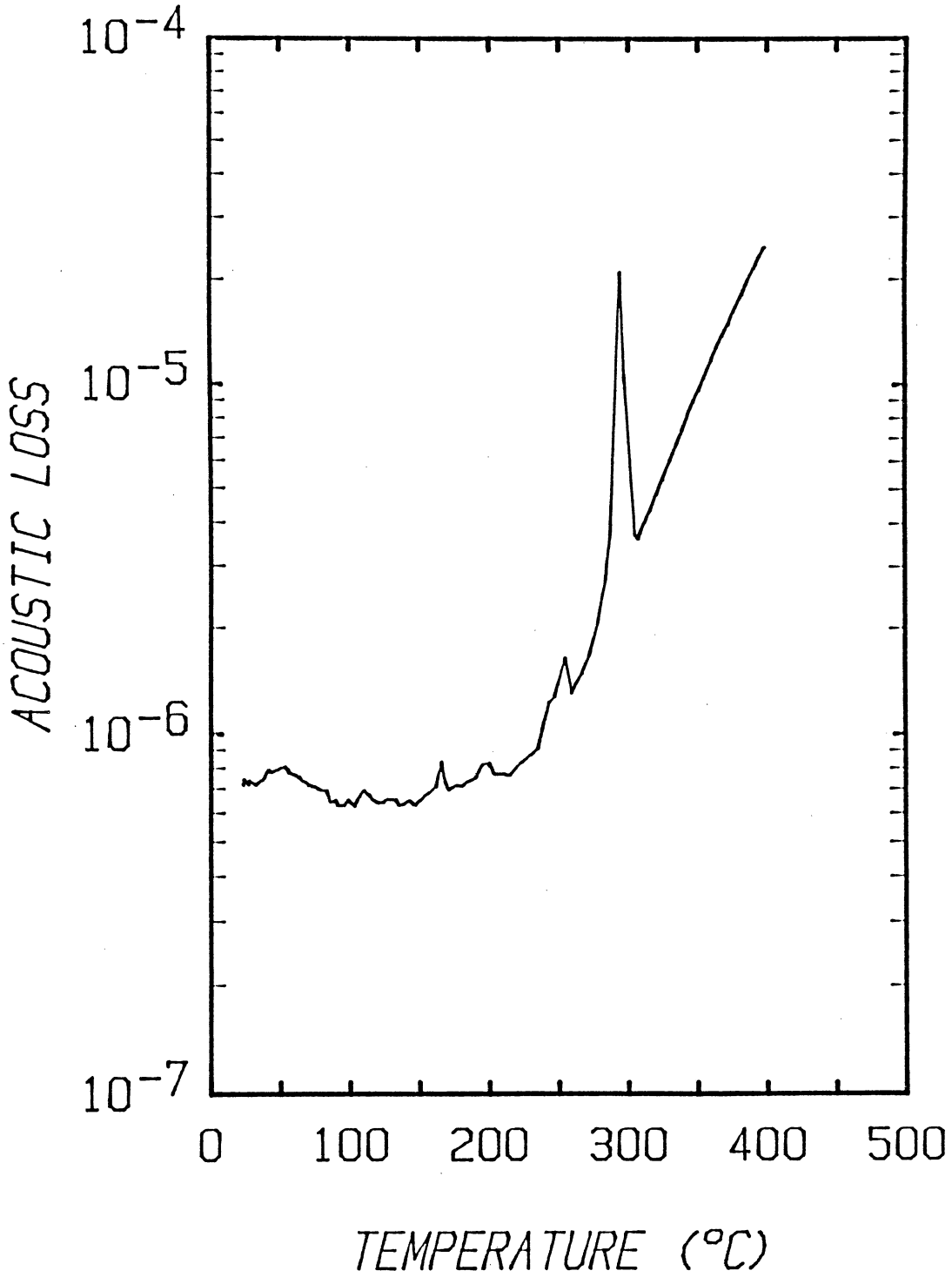

Figure 12. Background High Temperature Acoustic Loss of the Unswept D14-45 Sample.

under vacuum with the sample mounted in the sweeping apparatus before it was swept. The data shows an interfering mode at 325°C, a small peak at about 50°C, and an exponential increase in the loss at the higher temperatures. This loss spectrum is consistent with Fraser's results (8) on sodium doped sweeps-the loss increases exponentially as the temperature increases. Figure 13 shows the loss obtained during sweep number 7, the 18 hour hydrogen sweep. The solid curve is the loss obtained during warmup of the sample, and the dotted curve is the loss obtained during cooldown of the sample. The applied electric field was initially set at 1250 volts per centimeter, and during warmup the loss increased similarly as in the initial loss spectrum. The location of loss peaks in this spectrum differs from those of the initial spectrum because this data was taken with the sample in a hydrogen atmosphere where good thermal contact between the sample and the thermocouple was assured.

The loss from 8K to 100K after successive hydrogen sweeping to 404°C (sweeps 1 through 5) of D14-45, is shown in figure 14. Sweeps 4 through 7 are plotted in figure 15, and sweeps 7 through 9 are plotted in figure 16. All the loss values were calculated from the equivalent series resistance with a measured inductance of 8 Henrys. Most of the plots clearly show the 53K loss peak and what appears to be a loss peak near 25K. Since the 25K peak varies in a nondistinct fashion from plot to plot it is believed to be the result of interfering modes.

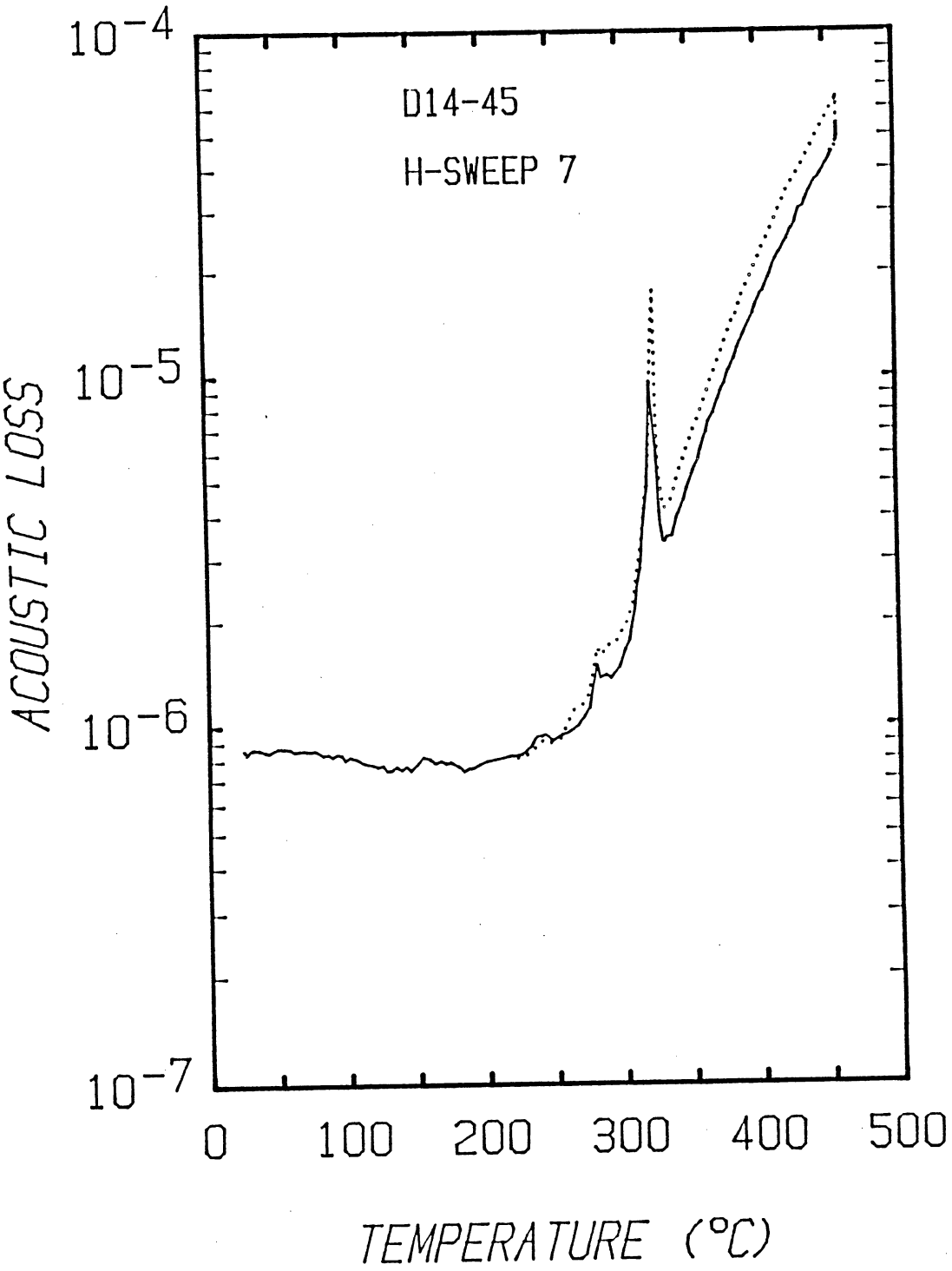

Figure 13. High Temperature Acoustic Loss of D14-45 Taken During Sweep Number 7.

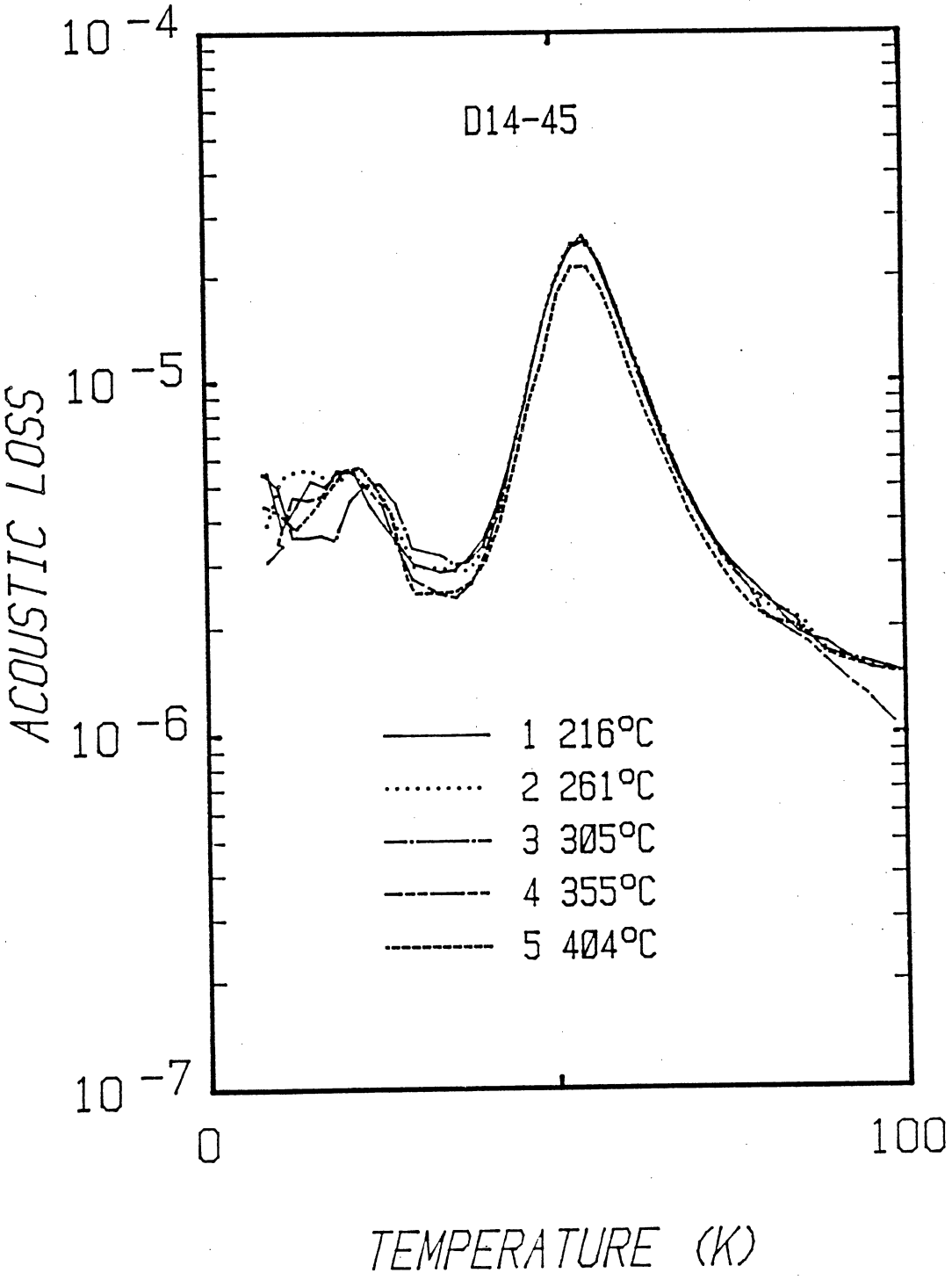

Figure 14. Low Temperature Acoustic Loss of D14-45 Taken After Sweeps 1-5.

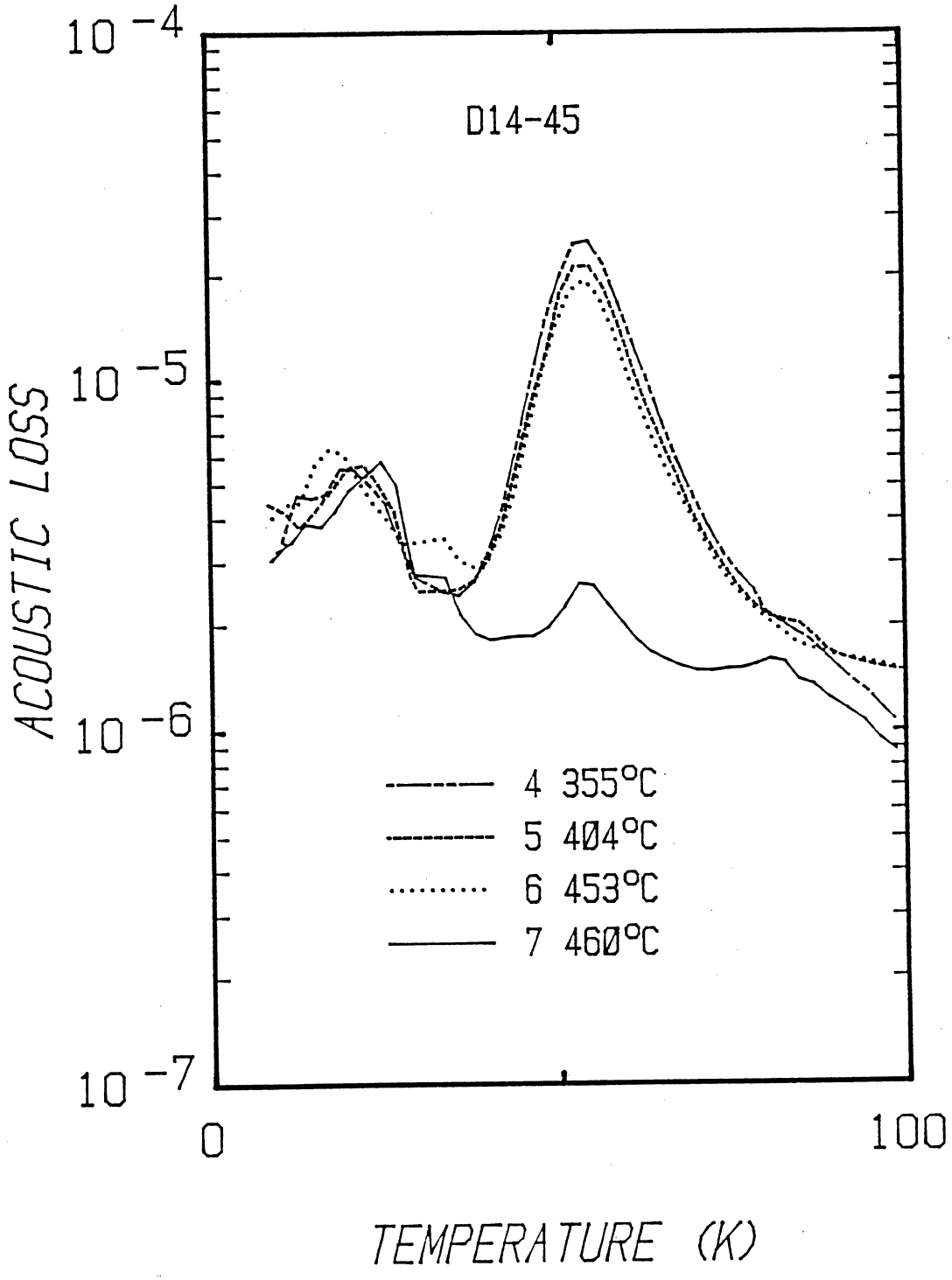

Figure 15. Low Temperature Acoustic Loss of D14-45 Taken After Sweeps 4-7.

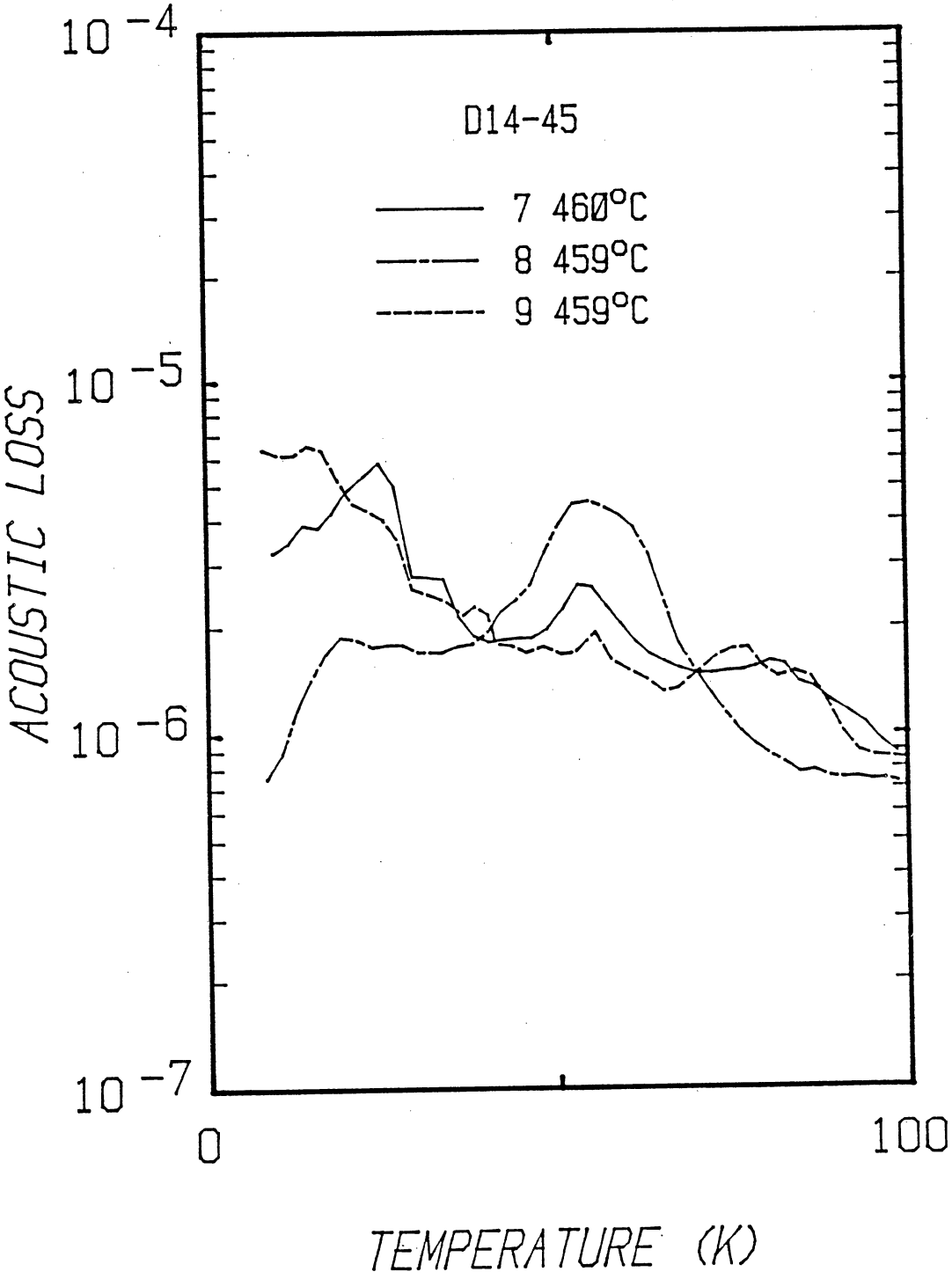

Figure 16. Low Temperature Acoustic Loss of D14-45 Taken After Sweeps 7-9.

The low temperature loss after sweep number 10 was obtained after removing the sample from the HC-40 holder and sweeping it with full electrodes for 10 hours at 459°C. The sample was oriented such that the electrical polarization was reversed relative to all previous hydrogen sweeps. After this sweep, the resonator was mounted in the HC-40 holder and the equivalent series resistance obtained from 8K to 100K. The sample was then swept for 20 hours (sweep number 9) with full electrodes. It was oriented as in sweeps 1 through 7.

Fraser (8) reported a decrease in the exponential character in the high temperature acoustic loss and a loss peak near 300°C for samples that have been swept in air. Comparison of figures 12 and 13 shows the exponential character did not change significantly during warmup. Since this sample was previously swept to 453°C (sweep 6) it was expected that the loss would decrease and a peak would appear as Fraser has reported. Since this was not the case, the applied electric field was increased to 2000 volts per centimeter and the temperature was held constant for 18 hours. As shown by the plot, the loss increased over this 18 hour period from 4.8×10^{-5} to 6.4×10^{-5}. However, this increase in the loss may be a result of the increase in the applied electric field.

A look at figure 15 shows the Al-Na^+ content decreased to 10% of its initial value during this sweep. Consequently, the data shows there was no decrease in the

loss above 250°C which was associated with a decrease in sodium compensated aluminum defect centers. However, there is a possibility that the logarithmic decrement system was encumbered by the HC-40 holder since it is, in part, made of silica.

The hydrogen sweep shown in figure 1 is that of a sample fabricated out of the same bar as the D14-45 sample. The current density during the first region of the sweep is shown in figure 17, and shows the peak's maximum temperature is about 375°C. The loss spectra of figure 14 indicates the concentration of Al-Na^+ centers was not affected by sweeping to temperatures ranging from 216°C to 355°C and a decrease in the loss was apparent only after sweeping to temperatures above 355°C. The strength of the loss peak after sweeping to 404°C indicates that very few sodium ions were removed from the aluminum sites and clearly shows that the current peak is not a result of the removal of the alkali ions from the aluminum defects.

The subsequent hydrogen sweeps, whose loss spectra are shown in figure 16, indicate that sodium is still present in the sample. The data shows an increase in the 53K loss peak that indicates some aluminum defect centers were not charge compensated with protons. This is unusual in that there was a decrease in sodium compensated aluminum defect centers, as shown by the 18 hour loss spectrum, and hydrogen sweeping is an irreversible process. The last sweep, also plotted in figure 16, indicates all aluminum defect centers

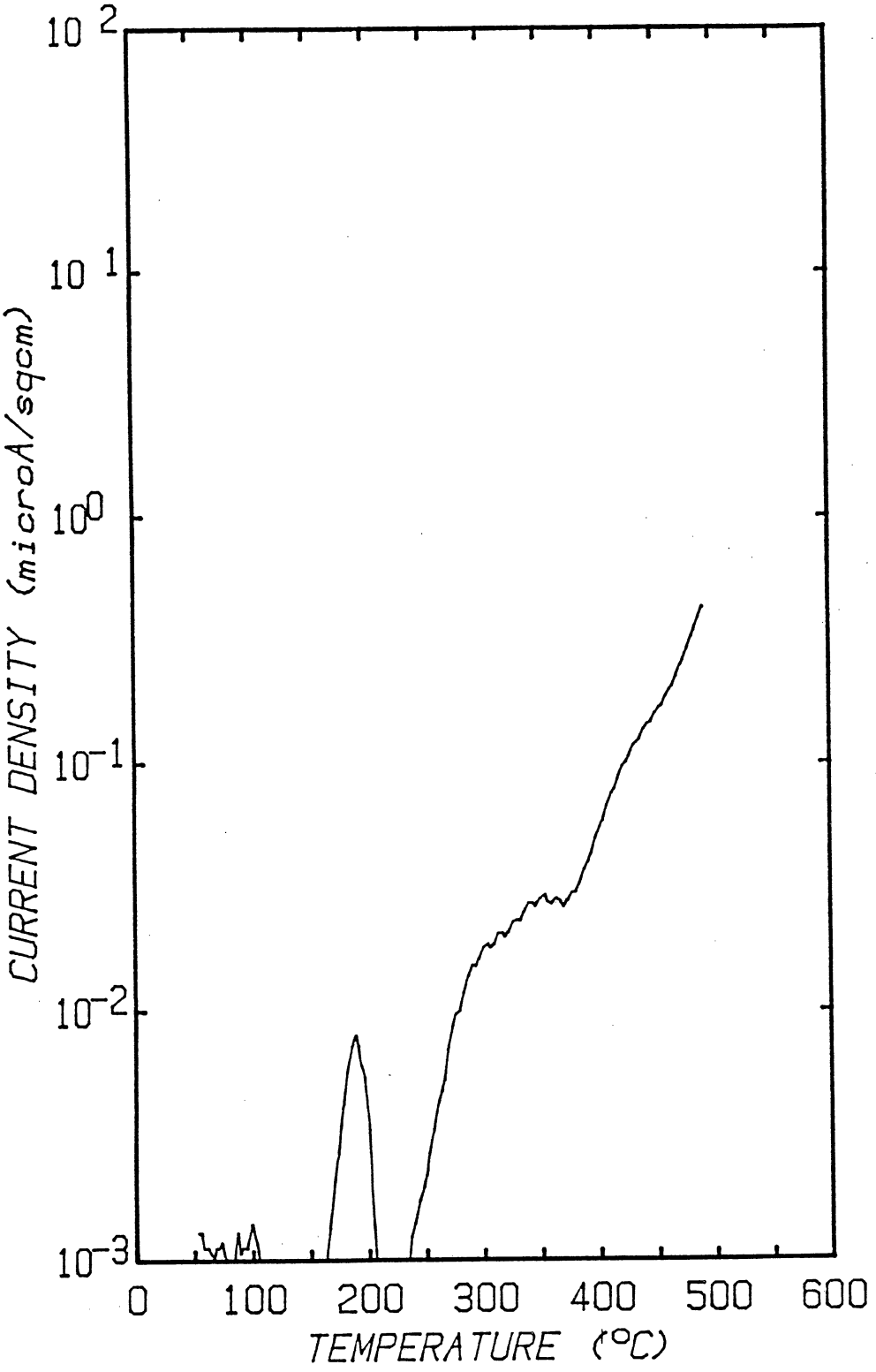

Figure 17. Current Density Versus Temperature of Hydrogen Sweep Shown in Figure 1. This sample was Fabricated Out of the Same Bar as the D14-45 Sample.

that were sodium compensated are no longer sodium compensated.

The increase in the low temperature loss spectra of the D14-45 sample after the 18 hour hydrogen swept indicate that the aluminum defects may not all be charge compensated with protons. Charge compensation may be with lithium ions that may have been adsorbed in the sweeping chamber during lithium sweeps done in the past and were freed from the chamber walls at the higher temperatures. However since the mobility of the lithium ion is high, compared to the mobility of protons, and the applied electric field was 1250 volts per centimeter, it is unlikely that charge compensation by the lithium ion is responsible for the decrease in the loss.

A possible picture of the current peak is that during electrodiffusion, with the sweeping electric field applied at room temperature, an opposing electric field is set up in the crystal between the aluminum site and the compensating ion. As the number of sites that become polarized increases, the observed current would increase and then decrease as all the sites became polarized. Observation of such an effect would reveal a current peak such as the one that is seen during the warmup phase of electrodiffusion and would account for the increase in the low temperature loss after reversing the electrical polarization of the sweeping field. Again this may be unlikely since the mobility of the sodium ion is greater than that of the proton.

CHAPTER V

CONCLUSIONS

Data correlation shows that the ion source creating the current peak during hydrogen electrodiffusion is not the charge compensating alkali from the aluminum defect center.

Since the samples used in this study were not hydrogen swept before fabrication, it is possible that the etch pipe tunnel concentration is high. Consequently, these tunnels are likely candidates for the ion source. However, a polarization of the aluminum and an accompanying alkali charge compensator or any substitutional and an accompanying interstitial could account for the current peak.

Though the high temperature acoustic loss data is inconclusive, the low temperature acoustic loss data indicate that in order to completely hydrogen sweep a sample, the electrodiffusion process must be carried out at temperatures greater than 375^{o}C and the temperature must be held constant for more than 18 hours. Since a characteristic of hydrogen sweeping is to remove the current peak, cycling a previously hydrogen swept sample to a temperature above the current peak's maximum temperature can be used as a check on sweeping effectiveness.

REFERENCES

(1) L. E. Halliburton, J. J. Martin, and D. R. Koehler, Precision Frequency Control, Vol. 1, Resonators and Filters, edited by E. A. Gerber and A. Ballato, (Academic Press, 1985).

(2) Y. Le Page, L. D. Calvert, and E. J. Gabe, J. Phys. Chem. Solids, 41, 721-725 (1980).

(3) T. Hanyu, J. Phys. Soc. Japan, 19, 1489 (1964).

(4) J. C. Brice, Rev. of Mod. Phys., 59, 105 (1985).

(5) G. Kreft, Rad. Effects, 26, 249 (1975).

(6) J. C. King, Bell Syst. Tech. J., 38, 583 (1959).

(7) A. Kats, Philips Res. Repts., 17, 133 (1962).

(8) D. B. Fraser, Physical Acoustics, Vol. 5, edited by W. P. Mason, (Academic Press, 1968).

(9) J. C. King and H. H. Sanders, IEEE Trans. Nucl. Sci., NS-19, 23 (1972).

(10) T. M. Flanagan and T. F. Wrobel, IEEE Trans. Nucl. Sci., NS-16, 130 (1969).

(11) P. Pellegrini, F. Euler, A. Kahan, J. M. Flanagan, and T. F. Wrobel, IEEE Trans. Nucl. Sci., NS-25, 1267 (1978).

(12) J. J. Martin, R. B. Bossoli, L. E. Halliburton, Brinda Subramaniam, and J. D. West, Proc. 37th Ann. Freq. Control Symp., 164 (1983).

(13) J. G. Gualtieri and J. R. Vig, Proc. 38th Ann. Freq. Control Symp., 42 (1982).

(14) L. E. Halliburtion, N. Koumvakalis, M. D. Markes, and J. J. Martin, J. Appl. Phys., 52, (1981).

(15) H. Jain and A. S. Nowick, J. Appl. Phys., 53, 477 (1982).

(16) T. M. Wilson, H. E. Halliburton, M. J. Jani, and J. J. Martin, Proc. 40th Ann. Freq. Control Symp., 26 (1986).

(17) J. Verhoogan, Am. Mineral., 37, 637 (1952).

(18) H. E. Wendon, Am. Mineral., 42, 859 (1957).

(19) W. P. Hanson, Proc. 38th Ann. Freq. Control Symp., 38 (1984).

(20) H. E. Bommel, W. P. Mason, and A. W. Warner, Phys. Rev., 99, 1894 (1955).

(21) H. E. Bommel, W. P. Mason, and A. W. Warner, Phys. Rev., 102, 64 (1956).

(22) J. C. King, Final Rept. DA36-039 SC-64586, Bell Telephone Lab., Inc., Whippany, New Jersey.

(23) A. S. Nowick and B. S. Berry, Anelastic Relaxation in Crystalline Solids, (Academic Press, 1972).

(24) J. J. Martin and T. M. Wilson, Oklahoma State University, 14 OCTOBER 1983, for the University of South Florida.

(25) Sawyer Research Products Inc., 35400 Lakeland Blvd., Eastlake, Ohio 44094.

(26) C. Y. Chen, Private Communication.

(27) Piezo Crystal Company, P. O. Box 619, Carlisle, Pennsylvania 17013.

(28) A. W. Warner, Bell System Technical J., 40, 1193 (1960).

(29) Motorola, Inc., P. O. Box 279, Carlisle, Pennsylvania 17013.

(30) KW Manufacturing Company, P. O. Box 508, Prague, Oklahoma 74864.

(31) Fotofabrication Corp., 3758 Belmont Ave., Chicago, Illinois 60618.

APPENDIX

DERIVATION OF MEANS TO CALCULATE CRYSTAL RESISTANCE R AND INDUCTANCE L

Dealing only with the series resonance of the crystal and considering the standard transmission circuit of the pi-network shown in figure 18a. The frequency synthesizer, counter, and vector voltmeter are connected to the pi-network via coaxial cable. With all grounds common the circuit can be redrawn as shown in figure 18b.

The left side of the circuit, left of the crystal, can be reduced to a voltage source and a single equivalent resistor by use of Thevinin's equivalent circuit theorem as shown figure 18c. Here

$$V_T = (R_2 V_a \angle 0^o)/(R_1+R_2),$$

where V_a is measured by the vector voltmeter, and

$$R_T = R_1 R_2/(R_1+R_2).$$

Considering the right side of the network, right of the crystal shown in figure 19a, and imagining the currents marked in the drawing, then I_1 is given by,

$$I_1 = V_b \angle \phi / R_L.$$

Where V_b is measured by the vector voltmeter and ϕ is the phase difference between points A and B. With V_2 given by,

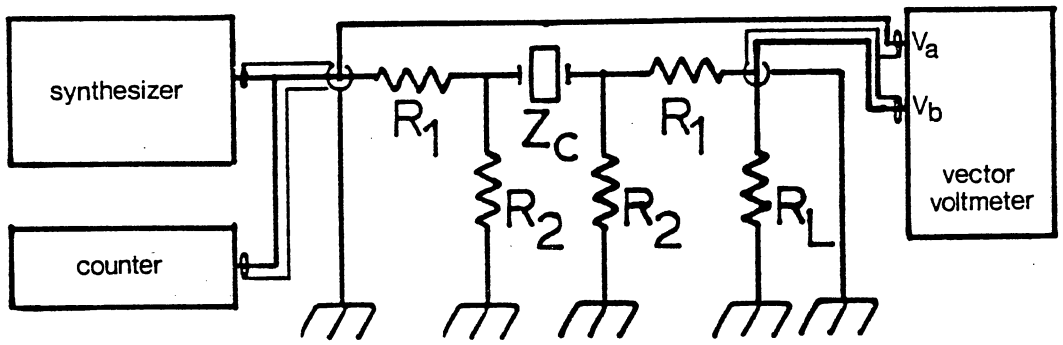

(a)

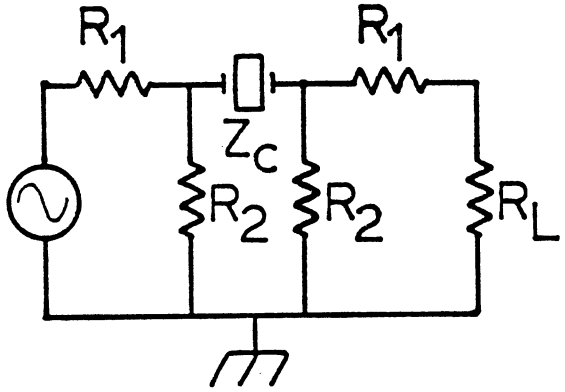

(b)

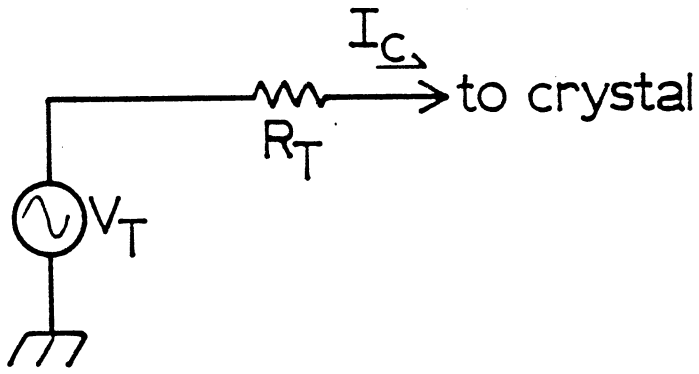

(c)

Figure 18. a) Transmission System. b) Equivalent Circuit of the Pi-Network. c) Electrical Equivalent of the Left Half of the Pi-Network.

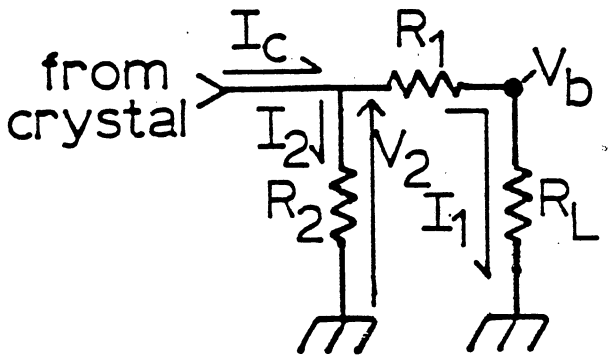

(a)

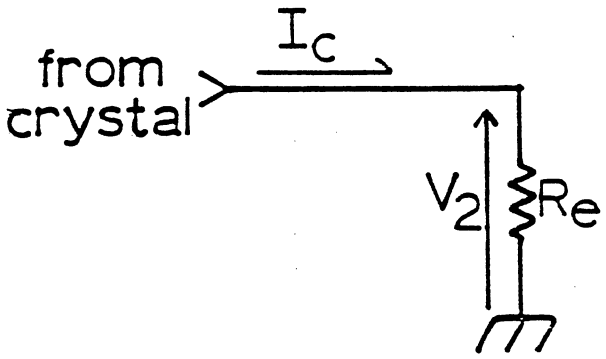

(b)

Figure 19. a) Right Half of the Pi-Network.
b) Electrical Equivalent of the Right Half of the Pi-Network.

$$V_2 = I_1(R_L+R_1),$$

substitution for I_1 results in

$$V_2=V_a\angle 0^o(R_L+R_1)/R_L.$$

By replacing this side of the circuit with the equivalent circuit shown in figure 19b with

$$R_e=R_2(R_1+R_L)/(R_1+R_2+R_L)$$

and $$I_c=V_2/R_e,$$

the pi-network can be replaced with the single loop, figure 20, where Z_c is the impedence of the crystal and

$$V_T=(R_T+Z_c+R_e)I_c.$$

Solving this expression for the crystal impedence,

$$Z_c=V_T/I_c-R_T-R_e$$

or, after substituting for V_T and I_c,

$$Z_c= (R_2R_LR_e)/[(R_1+R_2)(R_1+R_L)]\ V_a\angle 0^o/V_b\angle \phi\ -R_T-R_e.$$

At series resonance of the crystal both the phase angle ϕ and the reactance term of the crystal impedence equal zero. Thus, the crystal resistance R is given by

$$R = (R_2R_LR_e)/[(R_1+R_2)(R_1+R_L)]\ V_a/V_b\ -R_T-R_e.$$

Which is equation 8 of Chapter 1.

For the measurement of the inductance of the crystal, the series resonant frequency can be written

$$2\pi f_s=\omega_s.$$

From the reactance at resonance, the capacitance is given by

$$C=1/((2\pi f_s)^2L)$$

and the crystal impedence can be written as

$$Z= R+j2\pi fL(1-(f_s/f)^2).$$

By writing f as the sum of the series resonant frequency and

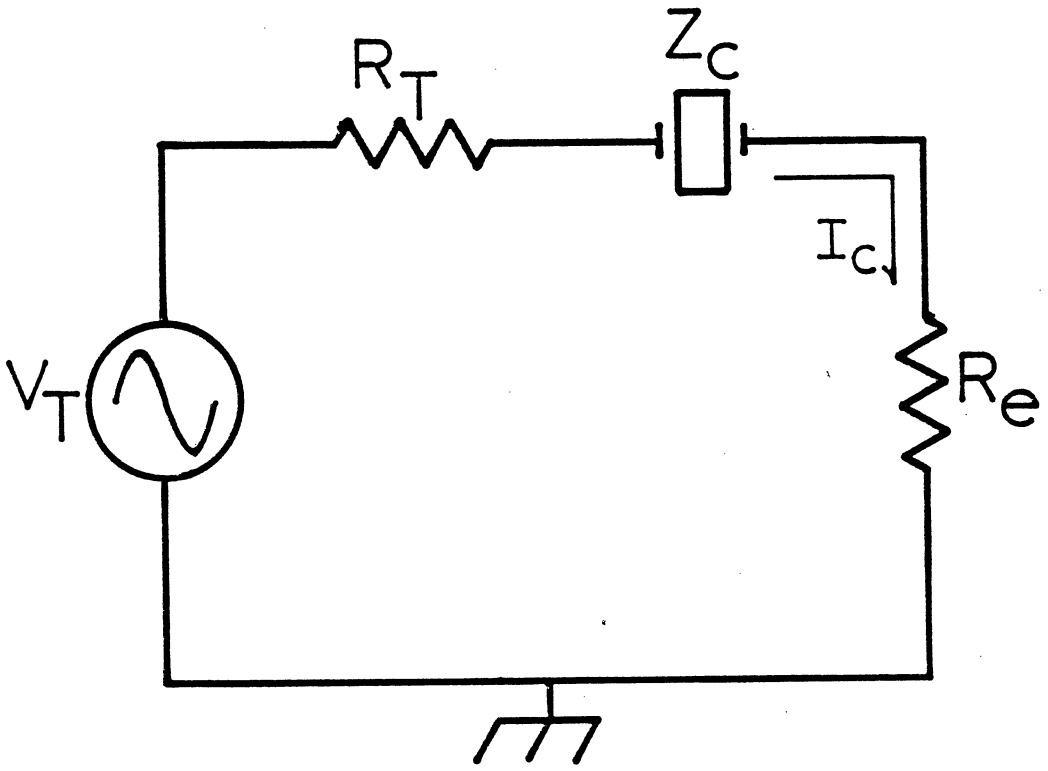

Figure 20. Equivalent Circuit of the Pi-Network.

an incremental frequency δ, then

$$Z= R+j2\ L(f_s+\delta)(1-1/(1+(\delta/f_s)^2)).$$

Expansion of the second term of the reactance and keeping only the first order terms in δ, the impedence is reduced to

$$Z= R+j4\pi\delta L.$$

Consequenty, a measurement of the crystal impedence while varying the frequency about the series resonant frequency of the crystal yields a straight line whose slope is $4\pi L$.

VITA

David Wayne Hart

Candidate for the Degree of

Master of Science

Thesis: A STUDY OF HYDROGEN ELECTRODIFFUSION IN ALPHA QUARTZ USING ACOUSTIC LOSS TECHNIQUES

Major Field: Physics

Biographical:

Personal Data: Born in Newton, Kansas, 8 December 1960, the son of Samuel C. and Delores S. Hart.

Education: Graduated from Weatherford High School, Weatherford, Oklahoma, May 1979; received Bachelor of Science degree in Engineering Physics from Southwesterm Oklahoma State University, Weatherford, Oklahoma, December 1984; completed requirements for the Master of Science degree at Oklahoma State University, May 1987.

Professional Experience: Laboratory Assistant, Department of Physics, Southwestern Oklahoma State University, August 1983, to December 1984; Teaching Assistant, Department of Physics, Oklahoma State University, January 1985, to May 1985; Research Assistant, Department of Physics, Oklahoma State University, June, 1985, to present.